bioRxiv preprint doi: https://doi.org/10.1101/2022.05.30.493970; this version posted May 30, 2022. The copyright holder for this preprint (which was not certified by peer review) is the author/funder, who has granted bioRxiv a license to display the preprint in perpetuity. It is made available under aCC-BY 4.0 International license.

HSPB5 disease-associated mutations have long-range effects on structure and dynamics through networks of quasi-ordered interactions

Christopher N Woods[1], Lindsey D Ulmer[2], Maria K Janowska[1], Natalie L Stone[1], Ellie I James[3,4], Miklos Guttman[3], Matthew F Bush[2], Rachel E Klevit[1]

[1]Department of Biochemistry, University of Washington, Seattle, United States
[2]Department of Chemistry, University of Washington, Seattle, United States
[3]Department of Medicinal Chemistry, University of Washington, Seattle, United States
[4]Molecular Engineering and Sciences Institute, University of Washington, Seattle, United States

Abstract

Small heat shock proteins (sHSPs) are chaperones whose importance in protein homeostasis is exemplified by dozens of missense mutations associated with tissue-specific disease states. Despite decades of studies, the structure, dynamics, and mechanism of chaperone activity remain unclear. Here we show that the human sHSP HSPB5 distinguishes native lens protein γD-crystallin from damaged γD-crystallin even though the mutant/damaged client is folded. The disordered N-terminal region of HSPB5 (NTR) is essential for its chaperone activity, whereas the structured domain (ACD) has no intrinsic activity. Nevertheless, two sHSP mutational hotspots associated with disease, D109 and R120, are located in the ACD. Our studies on wild-type HSPB5 oligomers reveal that distinct regions within the NTR interact with specific grooves presented on the ACD dimer and/or with other NTR sub-regions and that the number of binding partners is greater than the number of binding sites, leading to a large, but finite number of potential combinations of interactions at any given time. The ACD mutations result in increased dynamics and accessibility of the disordered NTR and enhanced chaperone activity in vitro. Our findings reveal that HSPB5 quasi-order is delicately balanced and that perturbations arising from mutations within the structured core cause alterations that contribute to misbalance in eye lens protein homeostasis that lead to cataract formation.

Introduction

Protein aggregation is a natural consequence of aging and must be controlled to maintain cellular health. Protein aggregates are a hallmark of multiple disease states in diverse tissues, including fibrillar aggregates associated with neurodegeneration and amorphous aggregates associated with cataract (Pedersen and Heegaard, 2013; Boatz et al., 2017). Small heat shock proteins (sHSPs) are a family of proteins whose ATP-independent chaperone activity contributes to protein homeostasis and inhibits protein aggregation (Horwitz, 1992). Although sHSPs were first discovered over 40 years ago (Ignolia and Craig, 1982), how the ten human sHSPs interact with diverse client proteins and how their chaperone activity is modulated remain poorly understood.

Previous studies have sought to gain insight into sHSP mechanisms by studying disease-associated mutations. Mutations identified in human sHSPs are primarily associated with autosomal dominant inheritance of tissue-specific diseases that include neuropathy, cataract, and myopathy (Datskevich et al., 2012). Among the first discovered and most extensively studied disease-associated mutations is substitution of Arginine 120 with Glycine in the ubiquitously expressed sHSP HSPB5, also

bioRxiv preprint doi: https://doi.org/10.1101/2022.05.30.493970; this version posted May 30, 2022. The copyright holder for this preprint (which was not certified by peer review) is the author/funder, who has granted bioRxiv a license to display the preprint in perpetuity. It is made available under aCC-BY 4.0 International license.

known as αB-crystallin (Vicart et al., 1998; Fardeau et al., 1978). HSPB5 R120G is associated with autosomal dominant inheritance of desmin-related myopathy and cataract in patients (Vicart et al., 1998). Mutations at the R120-equivalent residue in other human sHSPs are also associated with autosomal dominant inheritance of tissue-specific diseases, implying a common critical role for the residue (Datskevich et al., 2012). Arginine 120 is located in the conserved core domain that defines the sHSP family, called the α-Crystallin domain (ACD). The ACD is stably structured and forms a homodimer with a second copy of an ACD via long anti-parallel β-strands (Bagnéris et al., 2009). Arginine 120 is at the ACD dimer interface, where it can form an ionic interaction with Aspartate 109 (D109) across the dimer interface (Figure 1A). Intriguingly, patient mutations of HSPB5 D109 (D109H, D109A, D109G) are associated with similar phenotypes as R120G (Sacconi et al., 2012; Fichna et al., 2017; Brodehl et al., 2017). Expression of HSPB5 R120G in cells or animals is associated with formation of aggregates and/or eye lens defects, leading to the widely held belief that it is a less effective chaperone (Wu et al., 2018; Andley et al., 2011; Perng et al., 2004; Wang et al., 2001). *In vitro* characterizations have revealed that HSPB5 R120G has more exposed hydrophobic surfaces than WT, has faster subunit exchange dynamics (Liang and Liu, 2006), and is less effective at maintaining solubility of model client proteins under destabilizing conditions (Bova et al., 1999; Treweek et al., 2005). But the molecular details that underpin the deleterious consequences of the HSPB5 R120G mutation remain undefined.

The tissue-specificity of sHSP disease phenotypes implies that certain mutations are particularly deleterious under some conditions or toward some clients. To date, investigations of sHSP mutants suggest they form abnormal interactions with clients (Koteiche and Mchourab, 2006; Delbecq and Klevit, 2018). In light of the cataract-associated phenotype of HSPB5 R120G and D109H, we focused on one of the main eye lens client proteins, γD-crystallin. Mature lens fiber cells lack the ability to synthesize or degrade proteins, so lens proteins can accumulate damage over an individual's lifetime (Lynnerup et al., 2008). Failure to prevent aggregation of damaged proteins, including γD-crystallin and β/γ-crystallins, results in cataract, a leading cause of blindness worldwide (Foster, 2000). Lens cells are highly enriched in sHSP content where the total concentration of the two major lens sHSPs, HSPB4 and HSPB5 is roughly 150 mg/mL, corresponding to a subunit concentration of 7.5 millimolar.

Inherent properties of human sHSPs pose a major impediment to understanding their mechanisms. While sHSP protomers are small (~20 kDa), they assemble into large, structurally heterogenous and polydisperse ensembles of oligomers containing ~10-40 subunits that undergo dynamic subunit exchange among oligomers (Baldwin et al., 2011). There is high sequence conservation in the ACD, the only stably structured region (Figure 1A). ACDs form dimers that present grooves into which short sequences from termini can bind (Figure 3DEF, Clouser et al., 2019; Sluchanko et al., 2017; Clark et al., 2018; Klevit, 2020). The N- and C-terminal regions (NTR and CTR) are highly variable in sequence and length and are thought to support differences in client preferences and, possibly, mechanisms of activation.

We sought to identify determinants of HSPB5 chaperone activity by assessing changes caused by disease-associated mutations R120G and D109H. We compared the interactions, structure and dynamics, and chaperone activity of WT and mutant HSPB5 using hydrogen deuterium exchange coupled with mass spectrometry (HDX-MS) and biochemical assays and investigated interactions of the heterogenous NTR by Nuclear Magnetic Resonance Spectroscopy (NMR) and site-specific crosslinking. Paradoxically, the disease mutants associated with cataract and myopathy display gain-of-function properties, as they are more effective chaperones of a damaged lens client and associate with client

bioRxiv preprint doi: https://doi.org/10.1101/2022.05.30.493970; this version posted May 30, 2022. The copyright holder for this preprint (which was not certified by peer review) is the author/funder, who has granted bioRxiv a license to display the preprint in perpetuity. It is made available under aCC-BY 4.0 International license.

protein under conditions where the wild-type (WT) HSPB5 does not. Our results identify novel HSPB5 interactions that modulate binding to γD-crystallin and suggest a mechanism for premature cataract formation in patients with inherited mutations.

Results

Disease mutants of HSPB5 are activated chaperones of γD-crystallin, a major client in eye lens

Regions within HSPB5 responsible for its chaperone activity have not been determined for any physiological client. We sought this information for γD-crystallin ("GammaD"), a major client of HSPB5 in eye lens (Andley et al., 2014). In lens, pH values range from ~7 to ~6.5 and while non-lenticular tissues that express HSPB5 tend to have a pH of ~7.5, values can drop as low as 6.5 (Bassnett and Duncan, 1985; Mathias et al., 1991; Leem at al., 1999). HSPB5 is highly sensitive to pH in this range (Rajagopal et al., 2015a), so we investigated its capacity to delay aggregation of GammaD at the two extremes. WT, unmodified GammaD does not aggregate at 37 °C, so we used GammaD W130E, an oxidation-mimicking missense mutant that remains folded but spontaneously aggregates at 37 °C (Serebryany et al., 2016). At pH 6.5 and 37 °C, GammaD W130E aggregates over time as evidenced by increasing absorbance at 360 nm; the presence of HSPB5 WT delays the onset of aggregation by over two hours under assay conditions, even when GammaD W130E is present at 5-fold molar excess over HSPB5 (Figure 1B). To identify regions within HSPB5 that are required for the observed chaperone activity, we compared the activity of full-length HSPB5 to truncated versions that lack the NTR (HSPB5 ACD-CTR) or lack both the NTR and CTR (HSPB5 ACD-only). The results clearly demonstrate that the HSPB5 NTR is required, as neither the ACD-CTR construct nor the ACD-only construct have a detectable effect on the aggregation curve (Figure 1B). HSPB5 chaperone activity towards GammaD is greatly reduced at pH 7.5, providing only a short delay in aggregation onset at an identical molar ratio as the experiment conducted at pH 6.5 (Figure 1C). Co-incubation of HSPB5 WT and GammaD W130E at 37 °C under assay conditions resulted in soluble complexes that co-elute early on size exclusion chromatography (SEC), whereas no detectable complex was observed in the presence of GammaD WT (Figure 1D and Figure 1-figure supplement 2). Similar observations of activated chaperone activity of HSPB5 at low pH have been reported for aggregating proteins that are not thought to be physiological clients of HSPB5 (Rajagopal et al., 2015a). Our results indicate that the lower pH conditions in lens give rise to productive binding of aggregation-prone GammaD by HSPB5, resulting in enhanced chaperone activity ("activated").

HSPB5 mutations R120G and D109H are associated with cataract, suggesting they allow for enhanced aggregation in lens. Paradoxically, while their activity is similar to WT at pH 6.5 (Figure 1-figure supplement 1), we observe that unlike HSPB5 WT, both mutant forms are also highly effective chaperones at pH 7.5 (Figure 1C). Thus, the *in vitro* assays indicate a gain of function, at least under the higher pH condition. Consistent with this notion, both HSPB5 R120G and D109H formed soluble, long-lived complexes with GammaD W130E, but not GammaD WT, when co-incubated at 37 °C in pH 6.5 or 7.5 buffer (Figure 1-figure supplement 2). Both mutated sites are in the structured ACD, which does not itself have chaperone activity towards GammaD W130E (Figure 1B). Introduction of the R120G or D109H mutations into the ACD-only construct does not yield an active species (Figure 1-figure supplement 1). Together with the finding that HSPB5 chaperone activity against GammaD requires the NTR, the results suggest that functional client-interacting regions within the NTR are more available in R120G and D109H oligomers. This in turn implies that mutations in the structured ACD alter the properties and function of the sequence-distant and heterogenous NTR.

bioRxiv preprint doi: https://doi.org/10.1101/2022.05.30.493970; this version posted May 30, 2022. The copyright holder for this preprint (which was not certified by peer review) is the author/funder, who has granted bioRxiv a license to display the preprint in perpetuity. It is made available under aCC-BY 4.0 International license.

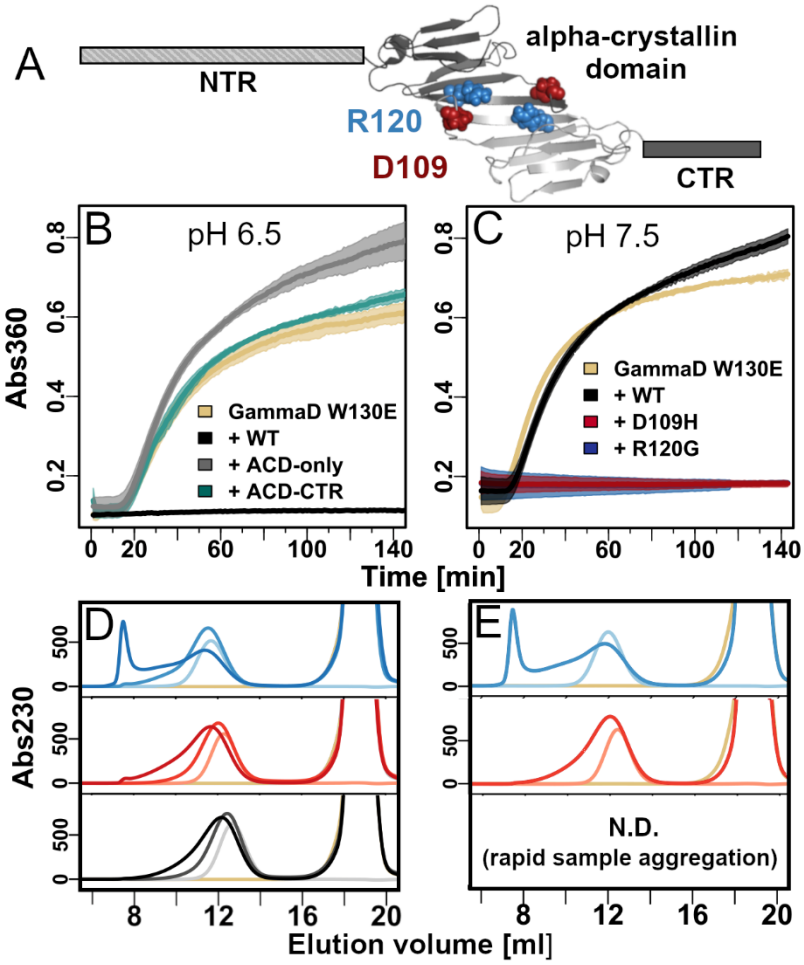

Figure 1. HSPB5 disease-associated mutants are activated chaperones against GammaD-crystallin W130E. A) Domain architecture of human HSPB5 N-terminal region (NTR), α-crystallin domain (ACD, PDB: 2N0K), and C-terminal region (CTR). Side chains of disease-associated mutation sites R120 (blue) and D109 (red) are shown as spheres. B) GammaD aggregation assay conducted at pH 6.5. 500 µM GammaD W130E (yellow) was incubated alone or in the presence of 100 µM HSPB5 WT (full length; black), HSPB5 ACD (gray), or HSPB5 ACD-CTR (cyan) at 37 °C. Aggregation was monitored by absorbance at 360 nm. C) GammaD aggregation assay conducted at pH 7.5. 500 µM GammaD W130E (yellow) was incubated alone or in the presence of 100 µM HSPB5 WT (black), HSPB5 D109H (red), or HSPB5 R120G (blue) at 37 °C. D) Size exclusion chromatography of co-incubated samples containing GammaD W130E and HSPB5. In each panel the lightest color trace is for 100 µM HSPB5 WT (grey), R120G (light blue), or D109H (light red) incubated at 37 °C for one hour at pH 6.5. Darker shades show samples co-incubated with 500 µM GammaD W130E for 1 hour (medium shade) or 3 hours (darkest shade). 500 µM GammaD W130E injected without pre-incubation is shown in yellow in all panels. E) Same as D but co-incubations were performed at pH 7.5 for 1 hour.

bioRxiv preprint doi: https://doi.org/10.1101/2022.05.30.493970; this version posted May 30, 2022. The copyright holder for this preprint (which was not certified by peer review) is the author/funder, who has granted bioRxiv a license to display the preprint in perpetuity. It is made available under aCC-BY 4.0 International license.

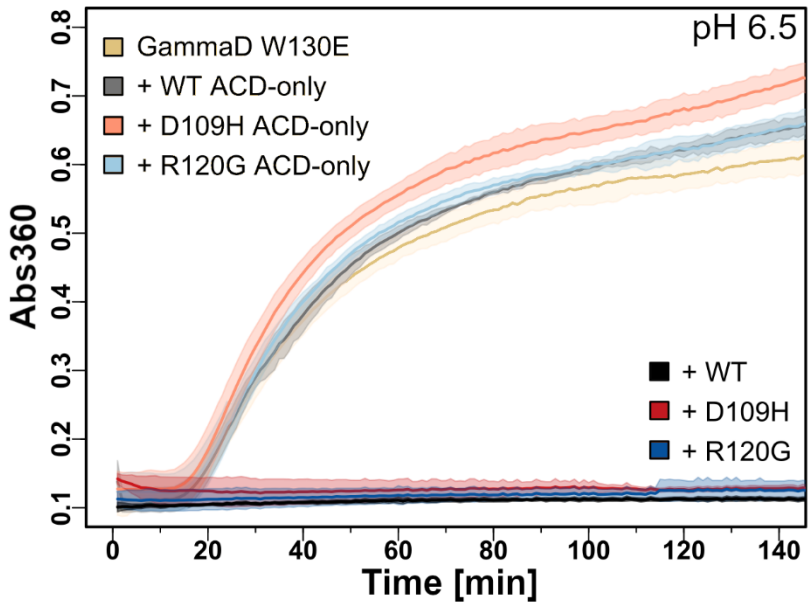

Figure 1-figure supplement 1. HSPB5 disease-associated mutations do not impart chaperone activity to the isolated ACD-only dimer. GammaD aggregation assay conducted in pH 6.5 buffer at 37 °C. All curves are replotted from main text figure 1B except D109H ACD (peach) and R120G ACD (sky blue).

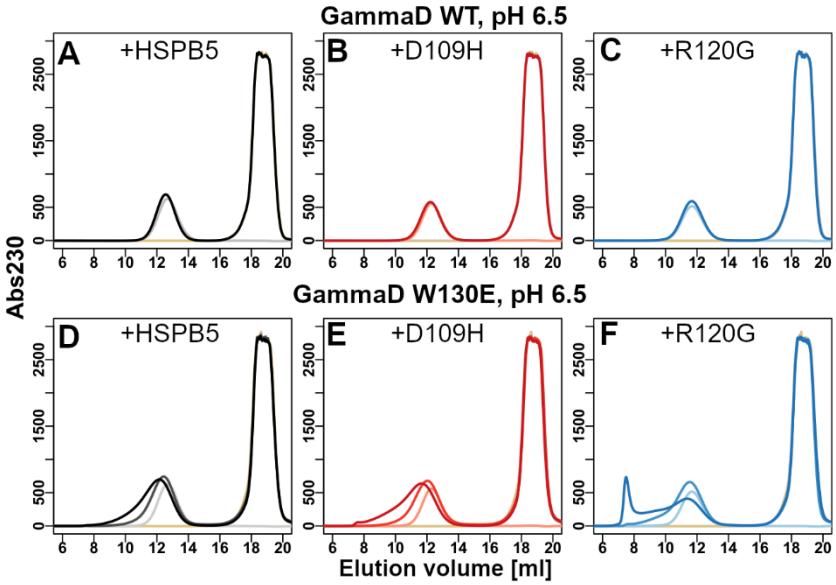

Figure 1-figure supplement 2. HSPB5 WT and disease-associated mutants bind destabilized but not WT GammaD. HSPB5 WT (A, black), D109H (B, red), or R120G (C, blue) were incubated alone or with GammaD WT for 3 hours at 37 °C in pH 6.5 buffer and then injected on a Superose6 column. Comparable data from co-elution experiments with GammaD W130E are plotted again below (same as Figure 1D).

bioRxiv preprint doi: https://doi.org/10.1101/2022.05.30.493970; this version posted May 30, 2022. The copyright holder for this preprint (which was not certified by peer review) is the author/funder, who has granted bioRxiv a license to display the preprint in perpetuity. It is made available under aCC-BY 4.0 International license.

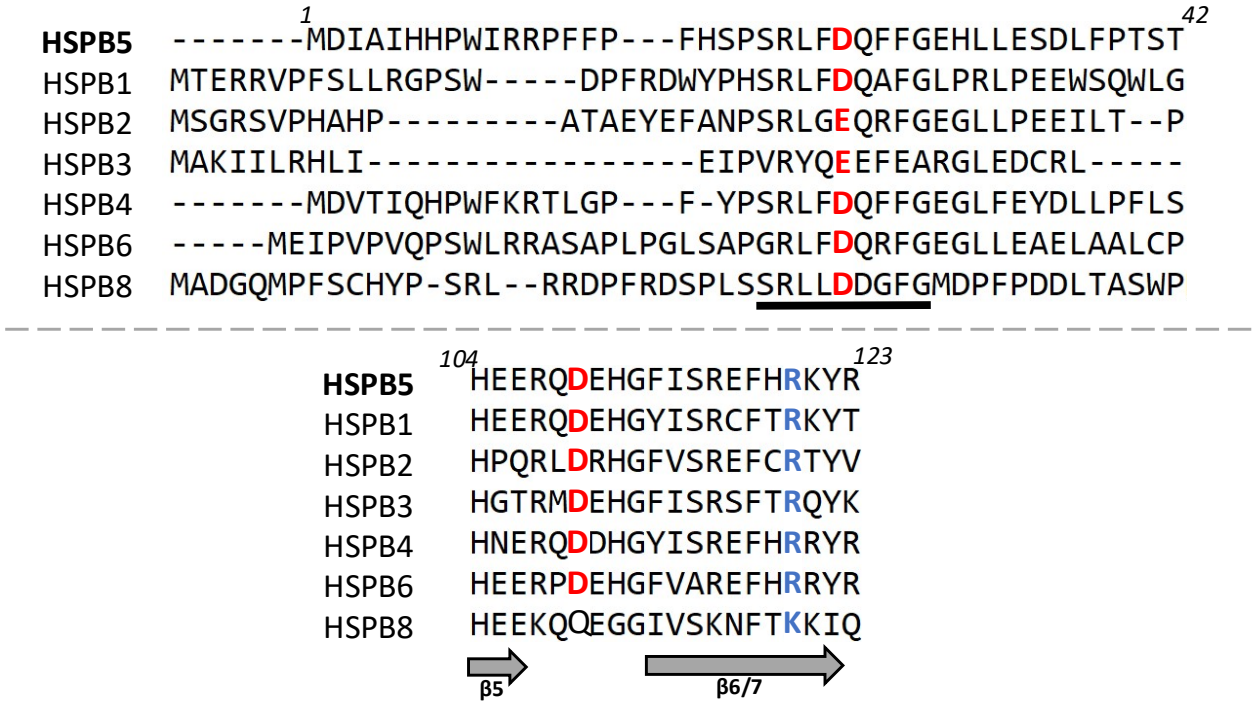

Figure 1-figure supplement 3. Alignment of human sHSP sequences. Alignment of human HSPB5, HSPB1, HSPB2, HSPB3, HSPB4, HSPB6, and HSPB8 amino acid sequences. The full sequence of each was used for alignment. HSPB5 residue numbers are shown above. Top, amino terminus through the N-terminal region Conserved sub-region, with the conserved sequence underlined in black and the aspartate that interacts with the ACD central groove highlighted in red. Bottom, region corresponding to HSPB5 ACD β-strands 5 and 6/7 with the positions of D109 (red) and R120 (blue) indicated.

Disease-associated mutations in ACD residues affect NTR structure and dynamics

To obtain insight into the structure and dynamics of HSPB5 as it exists in oligomers at pH 7.5, we used hydrogen deuterium exchange coupled with mass spectrometry (HDX-MS). HDX reports on the ability of protein backbone amides to exchange hydrogen with deuterium presented as $^{2}H_2O$. Positions that are in dynamic or unstructured regions exchange rapidly (seconds-minutes), while structured and hydrogen-bonded positions exchange slowly (hours-days) and are described as "protected." Thus, the degree of protection from exchange is indicative of local structure and dynamics. The experimental methodology provides peptide-level resolution and the extent of HDX for a given peptide reports on all backbone amides within that peptide except the two N-terminal residues of each peptide.

The three regions of HSPB5 are distinguishable in terms of their deuterium exchange behaviors (Figure 2A and B). The CTR exchanges fastest, with 100% of sites fully exchanged after 4 seconds at the extreme C-terminal end. This behavior is consistent with a dynamic and unstructured CTR in the context of HSPB5 oligomers. The lowest exchange rates are observed in the ACD, with some ACD-derived peptides incompletely exchanged after 20 hours (Figure 2-figure supplement 1). The slow exchange kinetics reflect the H-bond-rich β-sheet structure of the ACD. The NTR exhibits moderate exchange after 4 seconds, indicating that it is less dynamic than the disordered CTR and that it may be involved in

bioRxiv preprint doi: https://doi.org/10.1101/2022.05.30.493970; this version posted May 30, 2022. The copyright holder for this preprint (which was not certified by peer review) is the author/funder, who has granted bioRxiv a license to display the preprint in perpetuity. It is made available under aCC-BY 4.0 International license.

structures and/or interactions that slow amide exchange. By the 30 min timepoint, however, much of the NTR is fully exchanged, indicating that it is not as stably structured as the ACD. The general exchange profiles of the three regions of HSPB5 are similar to what has been reported for two other human sHSPs, HSPB1 and HSPB4 (Clouser et al., 2019; Kaiser et al., 2019), but in contrast to HSPB1 no evidence for bimodal deuterium uptake was observed for any peptide of HSPB5.

High coverage and resolution in the HDX data provide a detailed view of the NTR in the context of HSPB5 oligomers. At the 4 second timepoint, NTR peptides that span residues 1-54 exhibit exchange levels of roughly 35% - 60% and those more proximal to the ACD, whose structured residues begin at around residue 65, exhibit higher exchange levels, up to 68% (Figure 2A). Unlike HSPB1, whose NTR contains a sub-region that is completely exchanged at the 4 second timepoint, there are no fully-exchanged sub-regions within HSPB5's NTR after 4 seconds.

HDX time courses were collected for HSPB5 R120G and D109H (Figure 2-figure supplement 1 A-D). The overall exchange profiles are similar to WT, with the ACD exchanging slowest, the CTR exchanging fastest, and the NTR exhibiting intermediate exchange levels. Notable differences were observed at the peptide level in exchange time course plots (Figures 2C/D, Figure 2-figure supplement 1 A-D). Pairwise comparisons of uptake for each mutant, calculated as the difference in deuterium level between a peptide from the mutant and the corresponding peptide from the WT are shown for all timepoints (Figure 2-figure supplement 2 A-D). These snapshots reveal decreased protection in the NTR at early times (4 seconds, 1 minute) and in the ACD at longer times (30 minutes, 20 hours) for both mutants, with the magnitude of change being generally larger for D109H.

Focusing first on the mutation-harboring ACD, a majority of peptides exhibit higher exchange levels in the mutants at the 30-minute timepoint, consistent with global destabilization of the ACD (Figure 2D, Figure 2-figure supplement 2C). Peptides that contain residues 79-89 and 97-117 have the largest increase in exchange in both mutants, ranging around 20-30%. These regions are proximal to the two mutation sites (peptides containing the mutation sites were not compared because they have different sequences), so the observation implies that mutation at R120 affects the region near D109, and vice versa. The coupled effect is consistent with the putative salt bridge interaction between the two sidechains observed in some crystal structures (Bagnéris et al., 2009). Increased exchange of a long peptide that includes residues in the β6/7 strand that forms the dimer interface (i.e., residues 117-123) implies that the interface is more dynamic and/or slightly destabilized. In addition, two ACD loops, L3/4 (residues 83-90) and L8/9 (residues 137-143), have increased exchange at all exchange timepoints. These loops are proximal to one another and lead into and out of one side of the ACD edge groove (formed by β-strands 4 and 8, Figure 3-figure supplement 1). In sum, comparison of the 30-minute exchange profiles reveals that the two mutations affect the same regions within the structured ACD, but the magnitude of increased exchange is larger for D109H. Surprisingly, among the strongest effects are loops that link β-strands and lie on the edges of the β-sandwich ACD structure.

At the 4 second time point, exchange differences are most prevalent in the NTR, where deuterium uptake is increased for virtually every peptide derived from the two mutants (Figure 2C and Figure 2-figure supplement 2A). The overall patterns are quite similar for the two mutant proteins, although the magnitude of change is larger for peptides from D109H in general. The most distal N-terminal peptides are the least affected and are the most protected NTR peptides in the mutants (Figure 2C and Figure 2-figure supplement 1A). Peptides spanning residues ~20-55 have larger differences in

bioRxiv preprint doi: https://doi.org/10.1101/2022.05.30.493970; this version posted May 30, 2022. The copyright holder for this preprint (which was not certified by peer review) is the author/funder, who has granted bioRxiv a license to display the preprint in perpetuity. It is made available under aCC-BY 4.0 International license.

exchange relative to the WT protein (Figure 2-figure supplement 2). In both mutant oligomers, NTR peptides from the region that is proximal to the ACD display the highest exchange levels (Figure 2C and Figure 2-figure supplement 1A). Altogether, the HDX data are consistent with a destabilization/increase in dynamics in the ACD and increased accessibility/increased dynamics in the NTR, especially in the central region of the NTR.

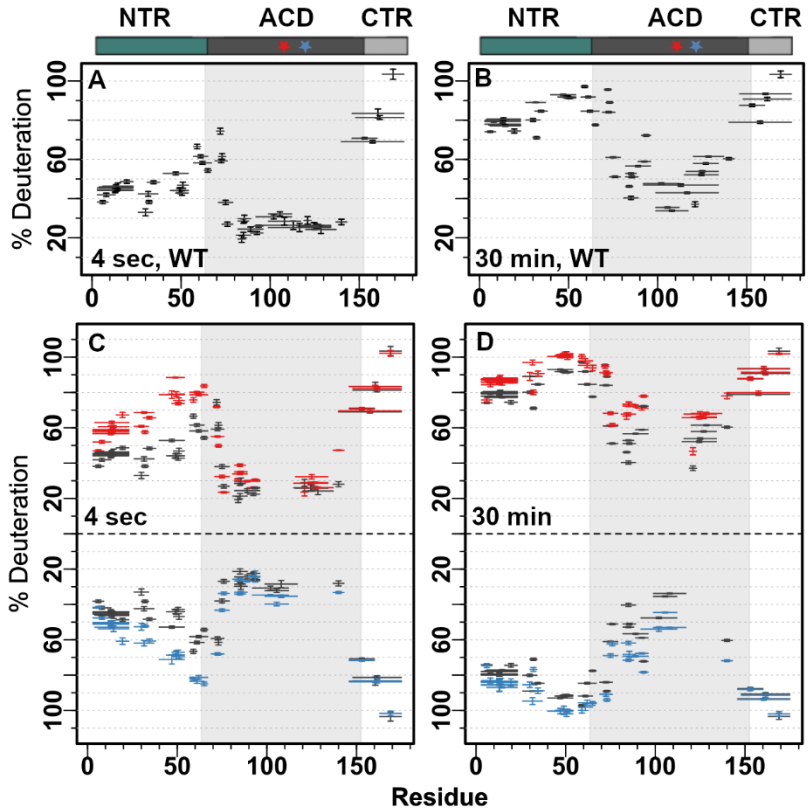

Figure 2. Hydrogen/Deuterium exchange reveals long-range effects of HSPB5 ACD mutations on oligomer structure and dynamics. A) Percent deuteration of HSPB5 WT at the 4 sec timepoint or B) 30 min timepoint relative to a fully deuterated control sample. Horizontal bars indicate exchangeable residues for each peptide, with the peptide center shown as a square. Y-axis error bars show standard deviation of all technical replicates. C) Percent deuteration of HSPB5 D109H (red, upper panel) or R120G (blue, lower panel) at the four second or D) 30 min timepoint. Data for HSPB5 WT are replotted in panels C and D (black). Domain boundaries are shown above the plots with ACD mutation sites marked with red (D109H) or blue (R120G) stars. The ACD boundaries are indicated in each plot by the gray inset.

bioRxiv preprint doi: https://doi.org/10.1101/2022.05.30.493970; this version posted May 30, 2022. The copyright holder for this preprint (which was not certified by peer review) is the author/funder, who has granted bioRxiv a license to display the preprint in perpetuity. It is made available under aCC-BY 4.0 International license.

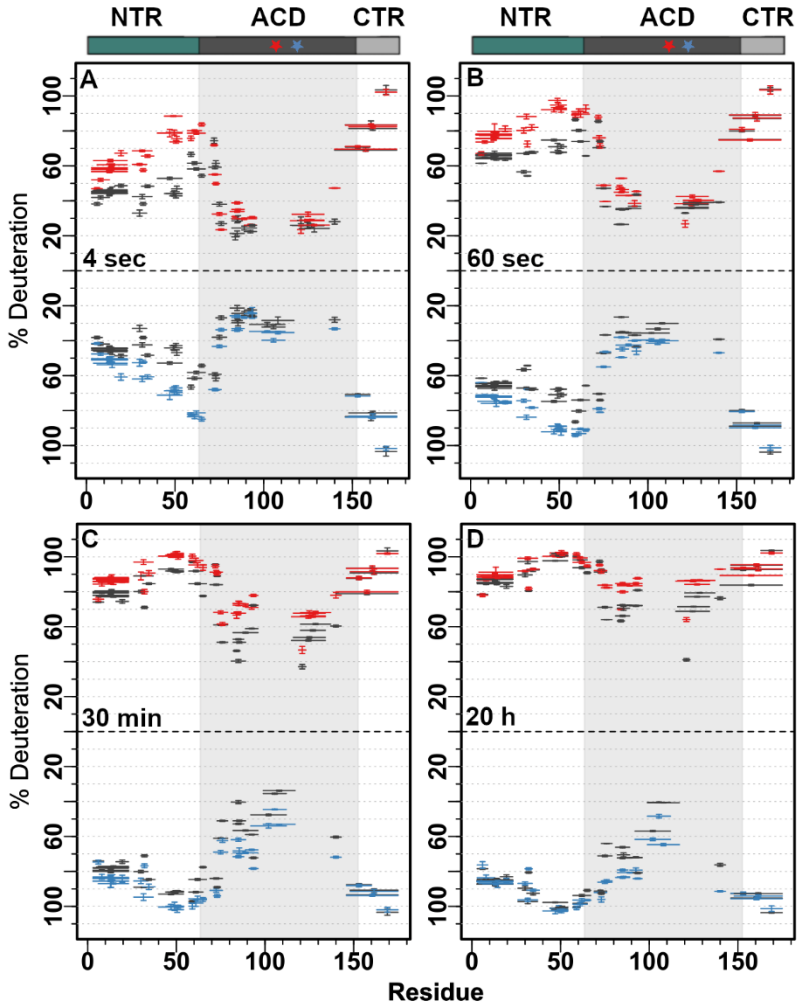

Figure 2-figure supplement 1. All Hydrogen/Deuterium exchange data for HSPB5 WT and mutants. Percent deuteration of HSPB5 WT (black), D109H (red), or R120G (blue) at the A) 4 second, B) 1 minute, C) 30 minute, or D) 20 hour time point. X-axis error bars indicate exchangeable residues for each peptide and the square denotes the peptide center. Y-axis error bars show standard deviation of all technical replicates.

bioRxiv preprint doi: https://doi.org/10.1101/2022.05.30.493970; this version posted May 30, 2022. The copyright holder for this preprint (which was not certified by peer review) is the author/funder, who has granted bioRxiv a license to display the preprint in perpetuity. It is made available under aCC-BY 4.0 International license.

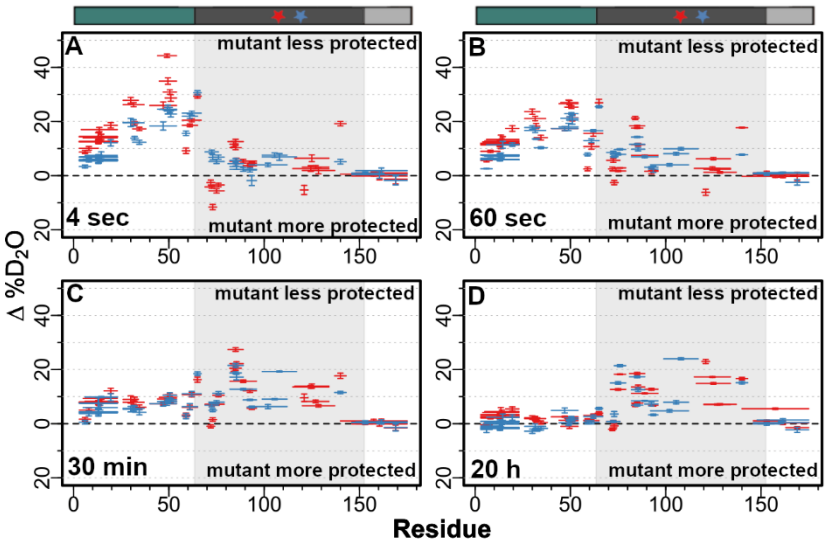

Figure 2-figure supplement 2. Change in percent deuteration relative to HSPB5 WT. Change in percent deuteration (calculated as mutant % Deuteration minus WT % Deuteration) versus HSPB5 residue number for the A) 4 second, B) 1 minute, C) 30 minutes and D) 20 hour time points. HSPB5 D109H is plotted in red, HSPB5 R120G is plotted in blue.

NTR sub-regions interact with ACD grooves

The observations that mutations in the ACD affect NTR HDX behavior imply an interplay between the NTR and ACD of HSPB5. As both the size and heterogeneity of full-length HSPB5 oligomers defy conventional structural analysis, we turned to the well-behaved, stably structured ACD-only dimer to assess its possible interactions with the NTR by solution NMR. On its own, the highly hydrophobic and heterogenous NTR is ill-behaved and has low solubility. We therefore divided the HSPB5 NTR into four sub-regions informed by the HDX data (and ultimately dictated by solubility) termed: Distal (residues 1-13), Aromatic (residues 11-22), Conserved (residues 17-34), and Boundary (residues 41-62; Figure 3-figure supplement 2). Synthetic peptides that correspond to each NTR sub-region were titrated into ^{15}N-labeled HSPB5 ACD-only and their effects on the Heteronuclear Single Quantum Coherence (HSQC) NMR spectrum were determined. Because we have previously assigned all features of the HSQC spectrum of the HSPB5 ACD-only dimer, perturbations in that spectrum provide residue-level information (Jehle et al., 2009). Each NTR sub-region exhibited distinct effects on the ACD spectrum. Only the Aromatic peptide produced no detectable perturbations to the HSPB5 ACD spectrum. The Distal and Conserved peptide titrations generated well-defined perturbations, while the Boundary peptide effects were quite weak (Spectra are shown in Figure 3-figure supplements 3 through 5).

Addition of the Distal peptide to HSPB5 ACD-only is accompanied by chemical shift perturbations (CSPs) and intensity losses in peaks corresponding to ACD edge groove residues (β-strands 4 and 8, Figure 3A and D; Figure 3-figure supplements 1 and 3). Smaller perturbations are detected in strands and loops proximal to the dimer interface. The Distal peptide has an Ile^{3}-Ala-Ile^{5} sequence similar to the "Ile-x-Ile" motif in the CTR of HSPB5 (Ile^{159}-Pro-Ile^{161}) that interacts with the edge groove (Delbecq et al., 2012). Comparison of Distal peptide effects to those for the known edge groove-binding

bioRxiv preprint doi: https://doi.org/10.1101/2022.05.30.493970; this version posted May 30, 2022. The copyright holder for this preprint (which was not certified by peer review) is the author/funder, who has granted bioRxiv a license to display the preprint in perpetuity. It is made available under aCC-BY 4.0 International license.

CTR peptide (HSPB5 residues 155-167) reveals that many of the same peaks are affected by both peptides (Figure 3B and E, Figure 3-figure supplement 3). The observed effects are consistent with both peptides binding in a similar manner with similar (low) affinity. There are therefore two edge groove-binding sequences per HSPB5 protomer, one in the NTR and one in the CTR, but only one edge groove. High local concentrations of termini in oligomers and similar apparent affinities for the NTR and CTR Ile-X-Ile motifs suggest there is likely competition between the CTR and Distal NTR for binding to an ACD edge groove.

Titration of the Conserved peptide yielded spectral perturbations consistent with a weak interaction (Figure 3C and F, Figure 3-figure supplement 4). Broadening is observed for peaks corresponding to residues located in the ACD central groove (β-strands 2, 3, and 6/7). Interactions involving the Conserved NTR sub-region and the ACD central groove have been observed in human HSPB1 and HSPB6, suggesting the interaction may be a common feature for all sHSPs (Clouser et al., 2019; Sluchanko et al., 2017). There are two Conserved sub-regions per HSPB5 dimer and only one central groove, leading to another situation in which there are more potential binding partners than there are binding sites.

The NMR results indicate that both the ACD edge and central grooves can harbor or sequester regions within the NTR. The ACD edge groove binds peptides that have an Ile-X-Ile motif and the ACD central groove binds the NTR Conserved sub-region. When observed in *trans* (i.e., as intermolecular interactions), the apparent affinities/lifetimes are quite modest. However, HSPB5 is present in millimolar concentrations in lens and local concentrations of potential interacting regions are expected to be even higher in HSPB5 oligomers. It is therefore likely that the interactions detected by NMR occur in the context of oligomeric HSPB5.

bioRxiv preprint doi: https://doi.org/10.1101/2022.05.30.493970; this version posted May 30, 2022. The copyright holder for this preprint (which was not certified by peer review) is the author/funder, who has granted bioRxiv a license to display the preprint in perpetuity. It is made available under aCC-BY 4.0 International license.

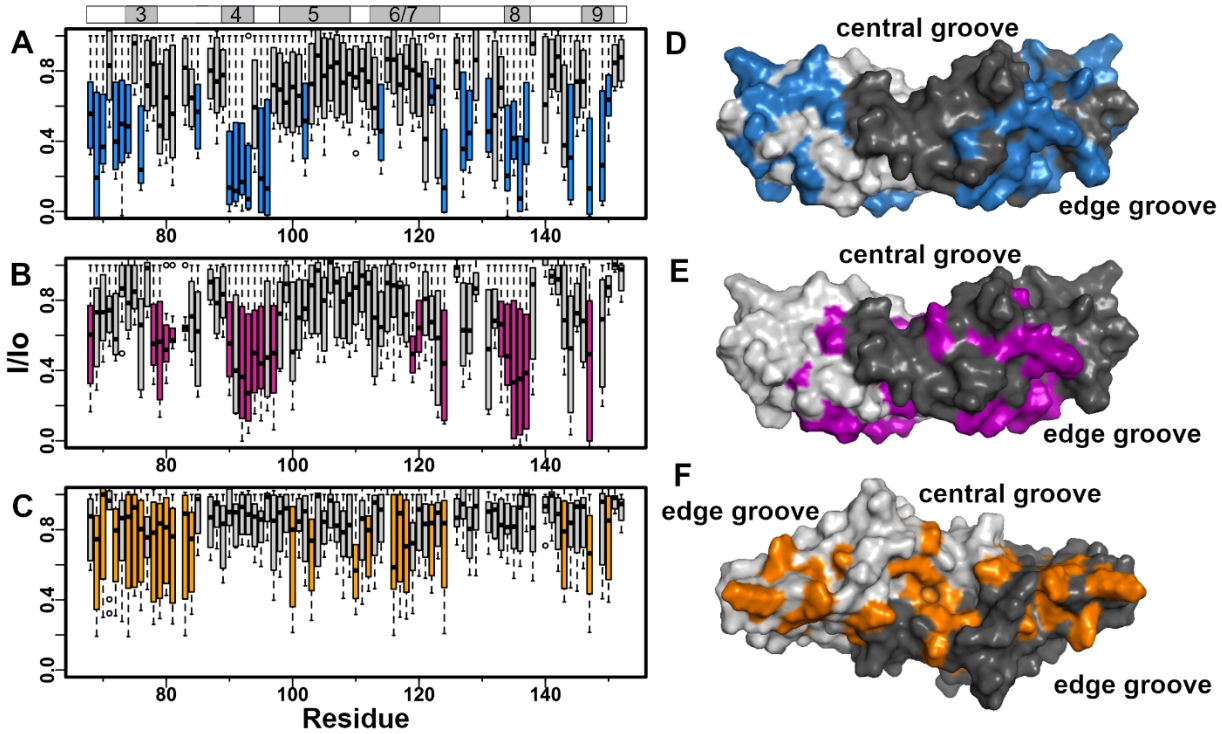

Figure 3. HSPB5 NTR-derived synthetic peptides interact with ACD grooves. Solution NMR was used to determine the effects of NTR-derived peptides titrated into samples containing ^{15}N-ACD-only dimer. NMR peak intensity of HSPB5 WT ACD-only in the presence of peptides relative to ACD-only alone (I/Io) versus HSPB5 ACD residue number is presented as box plots. The Distal (panel A, blue, residues 1-13), CTR (panel B, pink, residues 155-167), and Conserved (panel C, orange, residues 17-34) peptides generated perturbations that could be mapped to distinct surfaces on the ACD. Significant effects are plotted on the HSPB5 ACD-only structure (PDB 2N0K). Note that the ACD structure in panel C is rotated 90 degrees downward relative to the views in panels A and B.

bioRxiv preprint doi: https://doi.org/10.1101/2022.05.30.493970; this version posted May 30, 2022. The copyright holder for this preprint (which was not certified by peer review) is the author/funder, who has granted bioRxiv a license to display the preprint in perpetuity. It is made available under aCC-BY 4.0 International license.

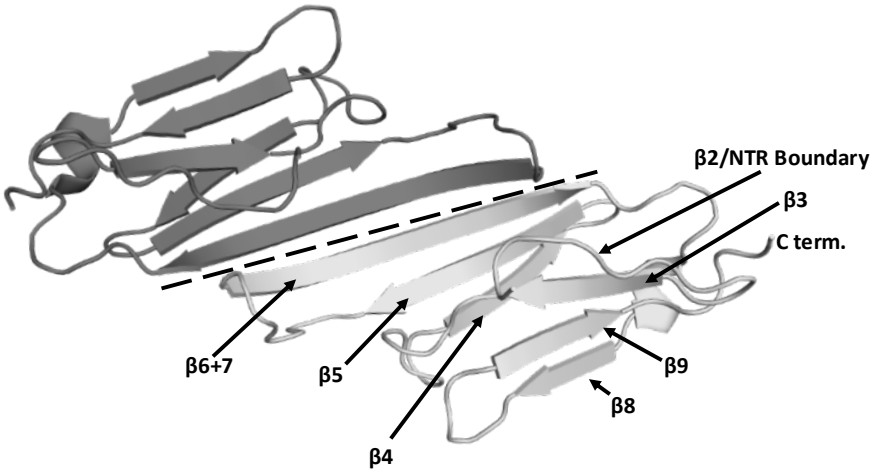

Figure 3-figure supplement 1. Structure of HSPB5 WT ACD-only dimer calculated from solution NMR restraints (PDB 2N0K, Rajagopal et al., 2015a). The dimer interface is marked with a dashed black line. Beta strands 2 through 9, which comprise the entirety of the ACD, are labeled. The N-terminal boundary and C-terminus are indicated.

bioRxiv preprint doi: https://doi.org/10.1101/2022.05.30.493970; this version posted May 30, 2022. The copyright holder for this preprint (which was not certified by peer review) is the author/funder, who has granted bioRxiv a license to display the preprint in perpetuity. It is made available under aCC-BY 4.0 International license.

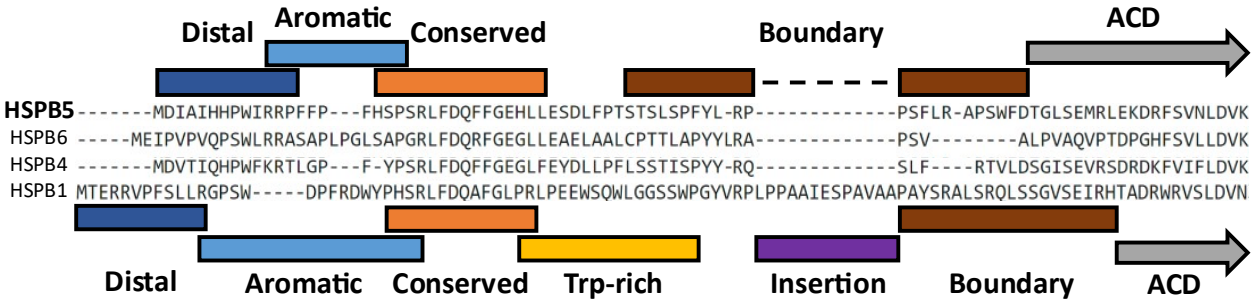

Figure 3-figure supplement 2. Alignment of human HSPB5, HSPB1, HSPB4, and HSPB6 N-terminal Region amino acid sequences created using Clustal Omega. HSPB5 NTR-derived synthetic peptides used in this study are shown above the sequence and HSPB1 NTR-derived synthetic peptides used in (Clouser et al., 2019) are shown below. The start of the ACD for HSPB5 and HSPB1 is indicated by a gray arrow.

bioRxiv preprint doi: https://doi.org/10.1101/2022.05.30.493970; this version posted May 30, 2022. The copyright holder for this preprint (which was not certified by peer review) is the author/funder, who has granted bioRxiv a license to display the preprint in perpetuity. It is made available under aCC-BY 4.0 International license.

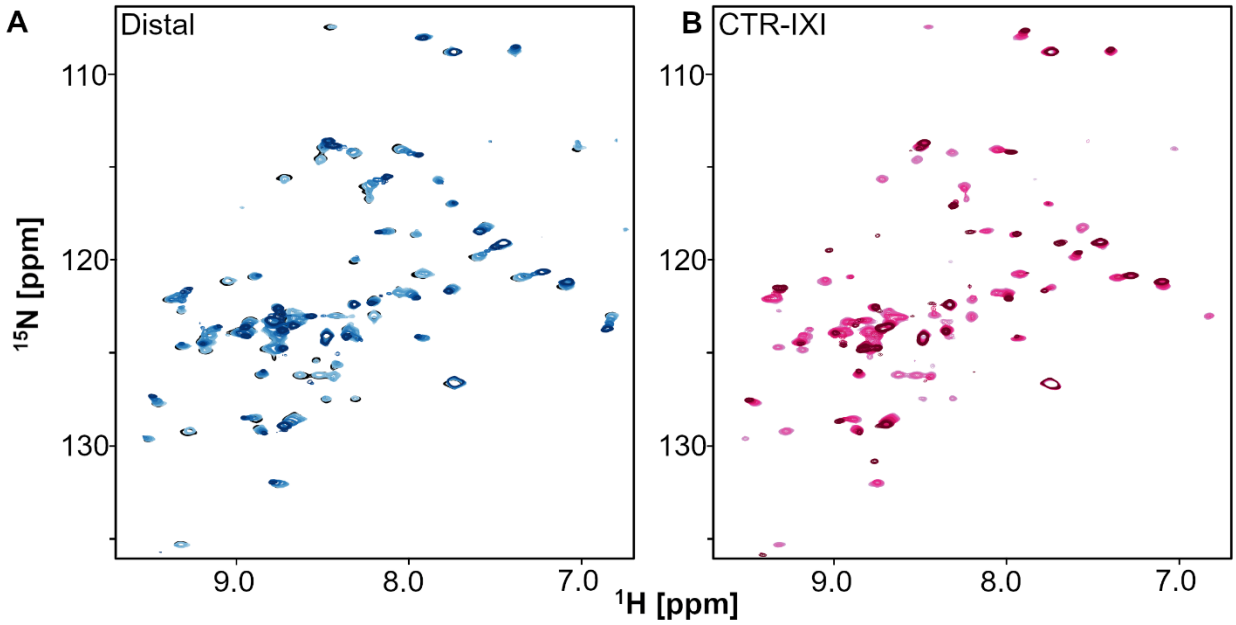

Figure 3-figure supplement 3. Titration series of 200 µM HSPB5 ACD-only WT in 25mM MOPS, 100mM NaCl, pH 7.5. A. Titration with 0.085, 0.1, 0.25, 0.5, 1, 2, and 3 molar equivalents of Distal peptide (HSPB5 residues 1-13). B. Titration with 0.05, 0.1, 0.25, 0.5, 1, 2, and 3 molar equivalents of CTR-IXI peptide (HSPB5 residues 155-167). ACD-only with no peptide added is shown in black, then increasing amounts of peptide are shown in a gradient from light color to dark. All titration points contain less than 1% DMSO (v/v).

bioRxiv preprint doi: https://doi.org/10.1101/2022.05.30.493970; this version posted May 30, 2022. The copyright holder for this preprint (which was not certified by peer review) is the author/funder, who has granted bioRxiv a license to display the preprint in perpetuity. It is made available under aCC-BY 4.0 International license.

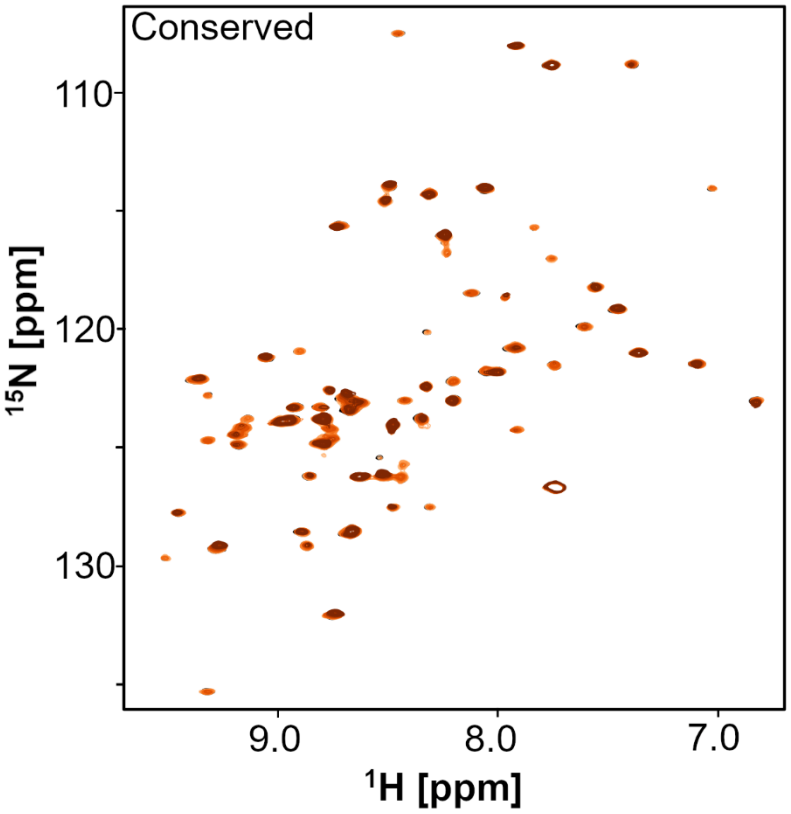

Figure 3-figure supplement 4. Titration series of 200µM HSPB5 ACD-only WT in 25mM MOPS, 100mM NaCl, pH 7.5. A. Titration with 0.05, 0.1, 0.25, 0.5, 1, 2, 3, and 4 molar equivalents of Conserved peptide (HSPB5 residues 17-34). ACD-only with no peptide added is shown in black, then increasing amounts of peptide are shown in a gradient from light color to dark. All titration points contain less than 1% DMSO (v/v).

bioRxiv preprint doi: https://doi.org/10.1101/2022.05.30.493970; this version posted May 30, 2022. The copyright holder for this preprint (which was not certified by peer review) is the author/funder, who has granted bioRxiv a license to display the preprint in perpetuity. It is made available under aCC-BY 4.0 International license.

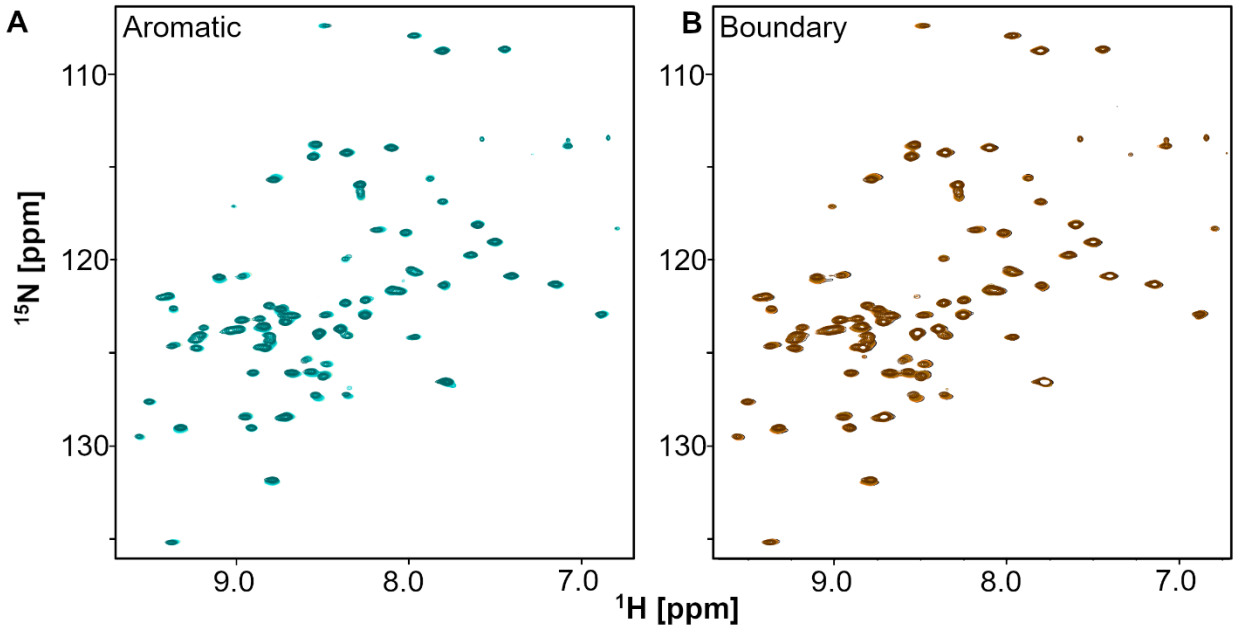

Figure 3-figure supplement 5. Titration series of 200uM HSPB5 ACD-only WT in 25mM MOPS, 100mM NaCl, pH 7.5. A. Titration with 0.25, 0.5, 1, 2.5, and 5 molar equivalents of Aromatic peptide (HSPB5 residues 11-22). B. Titration with 0.25, 0.5, 1, and 2.5 molar equivalents of Boundary peptide (HSPB5 residues 41-62). ACD-only with no peptide added is shown in black, then increasing amounts of peptide are shown in a gradient from light color to dark. All titration points contain less than 1% DMSO (v/v).

NTR sub-regions interact with other NTR sub-regions

To further identify interactions that occur in the context of HSPB5 oligomers, we adopted a targeted cross-linking/mass spectrometry strategy. Common chemical cross-linking reagents can span many tens of Å and only react with specific reactive amino acids that are solvent accessible. To circumvent these issues, the non-canonical amino acid p-benzoyl-l-phenylalanine (BPA) was installed at single positions in HSPB5 using amber codon suppression (Chin et al., 2002). When excited at ~360 nm, the benzophenone moiety of BPA forms covalent crosslinks to C-H bonds that are within 2.5-3.1 Å, providing a powerful probe for proximity/atomic contacts (Dorman and Prestwich, 1994). To minimize perturbation, we installed BPA at aromatic sites within the NTR to investigate NTR interactions in HSPB5 oligomers.

As proof-of-principle, we installed BPA within the Distal NTR sub-region, as the NMR results identified its binding site as the ACD edge groove. In sHSPs, Ile-X-Ile interactions occur via a “knob in hole” mechanism, in which a methyl group of each isoleucine “knob” inserts into a hydrophobic “hole” in the ACD edge groove (Delbecq et al., 2012). To minimize possible perturbations due to introduction of the large, aromatic BPA sidechain, Trp9, four residues removed from the putative NTR edge groove-binding motif, was chosen as the site of BPA incorporation. Oligomers composed of W9BPA-HSPB5 were irradiated at 360 nm for 30 minutes at 4 °C. SDS-PAGE analysis of the resulting samples revealed a major product that runs at the expected position of a covalent HSPB5 dimer (i.e., singly cross-linked species), with similar amounts of higher order species representing >2 crosslinked subunits detected (Figure 4-

bioRxiv preprint doi: https://doi.org/10.1101/2022.05.30.493970; this version posted May 30, 2022. The copyright holder for this preprint (which was not certified by peer review) is the author/funder, who has granted bioRxiv a license to display the preprint in perpetuity. It is made available under aCC-BY 4.0 International license.

figure supplements 1 and 2). We performed in-gel digests of the covalent dimer band and subjected the resulting peptides to mass spectrometry. Data-dependent fragmentation and bioinformatic analysis of the resulting spectra led to the identification of multiple HSPB5 regions to which BPA at position 9 is cross-linked (Figure 4A). The region with the highest number of peptide spectral matches (PSMs) is the ACD edge groove, at and around residue 138 and around residue 85, confirming the Distal-to-edge groove interaction implied by the solution NMR results. Importantly, the number of PSMs is not a quantitative metric related to the prevalence of a given interaction. In addition, crosslinks to several NTR sub-regions were identified. Notably, the crosslinks are not randomly distributed throughout the NTR but are more localized. The highest density of crosslinks within the NTR is to residues between ~60-70. These include the C-terminal part of the Boundary region and the first structured residues of the ACD; the latter were perturbed in the NMR distal peptide titration (Figure 3A and D). Cross-links were also detected to Conserved sub-region residues 25-32, the Boundary sub-region residues 38-50, and to the Distal sub-region itself. UV-exposed HSPB5 molecules that migrate as dimers on SDS-PAGE must contain a covalent cross-link between two chains. As all chains contained a BPA, it is also possible that some identified cross-links may be intra-chain. However, MS analysis of material that migrated at the position of monomeric HSPB5 in UV-treated samples (and could in principle contain intra-chain cross-links) did not identify cross-links, indicating that intra-chain crosslinks are rarely formed. Thus, incorporation of BPA at Trp9 both confirmed that the Distal sub-region interacts with ACD edge grooves in a neighboring protomer and revealed novel inter-NTR interactions within HSPB5 oligomers.

To discover additional NTR interactions, BPA was individually installed at NTR positions F24, F47, and F61. Of these, F24BPA produced the smallest number of identified cross-links and F61BPA produced the highest number (Figure 4B-D). Cross-links were observed to the ACD, specifically to the edge groove, from F47BPA. Although the peptide containing F47 (Boundary) produced NMR perturbations when added to the ACD, they were too weak to assign to specific regions. Thus, the BPA cross-linking results identify a third region of HSPB5 that visits the ACD edge groove. The only other ACD residues that had detectable cross-links in any of the BPA species analyzed are at the N-terminal end of the structured ACD, around residues 65 through 70. BPA installed at positions W9 (see above), F24, and F61 generated such cross-links. In the solution NMR structure of HSPB5 ACD (PDB 2N0K) residues 66-71 form a β2 strand that forms part of the ACD central groove. These residues were distinctly perturbed upon addition of the Conserved peptide (residues 17-34) in NMR titrations, again demonstrating agreement between the in *trans* NMR data and the in-oligomer cross-linking data. Finally, NTR-to-NTR cross-links were observed for all BPA species. Cross-links from BPA sites 24 and 61 to the Aromatic sub-region (residues 11-22) are notable, as this peptide showed no evidence of an ACD interaction and is therefore likely to interact primarily with NTR sub-regions. Altogether, the BPA crosslinking data both confirm interactions inferred from NMR experiments and identify numerous novel interactions that involve the NTR in heterogeneous, polydisperse oligomers. The new interactions involving the NTR greatly expand the limited information obtained from past solid-state NMR, cryo-EM, and biochemical studies (Jehle et al., 2011; Peschek et al., 2013; Ghosh and Clark, 2005).

bioRxiv preprint doi: https://doi.org/10.1101/2022.05.30.493970; this version posted May 30, 2022. The copyright holder for this preprint (which was not certified by peer review) is the author/funder, who has granted bioRxiv a license to display the preprint in perpetuity. It is made available under aCC-BY 4.0 International license.

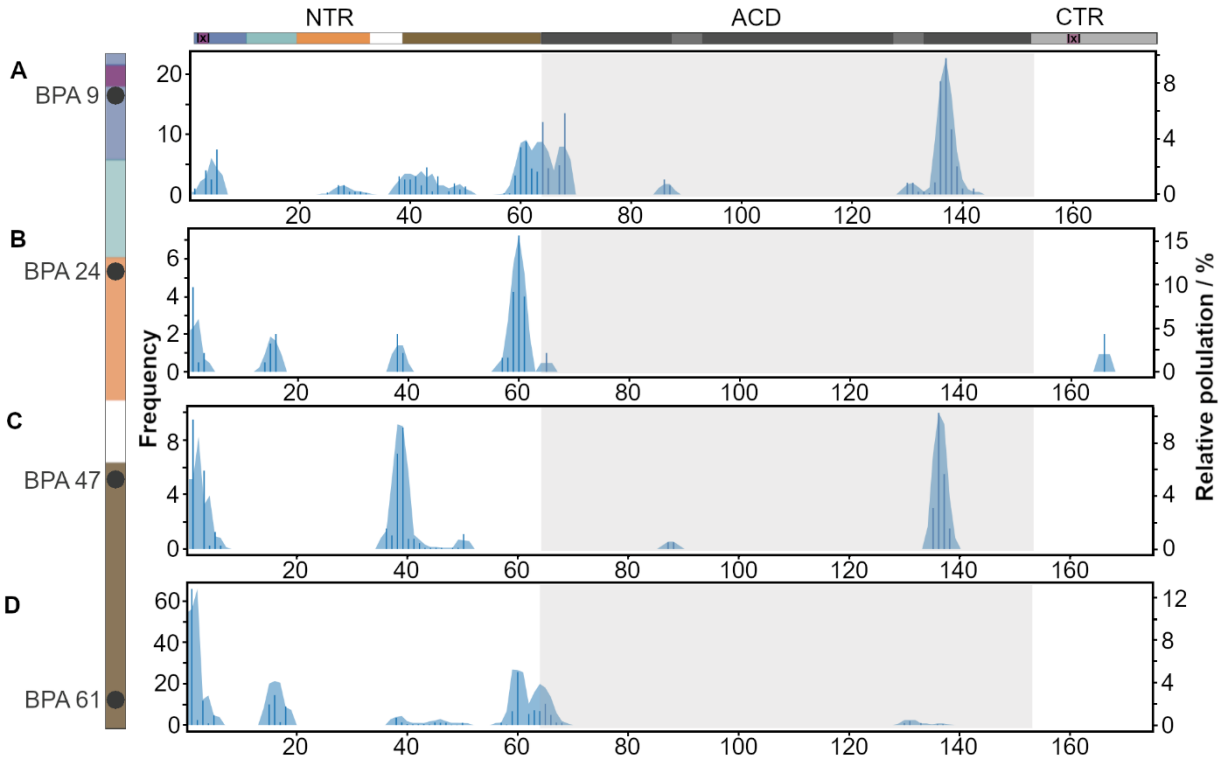

Figure 4. BPA cross-linking reveals HSPB5 NTR interactions. Amber codon suppression was used to install the photo-activatable cross-linker p-benzoyl-l-phenylalanine (BPA) in full length HSPB5 at residues A) 9, B) 24, C) 47, or D) 61. Cross-links formed between BPA and other sites in HSPB5 are shown in blue. Bars indicate the total number of peptide spectral matches for each crosslink identified and blue shading shows the relative number of crosslinks in a 3-residue sliding window. HSPB5 domain boundaries are shown and NTR sub-regions are colored for the Distal (dark blue), Aromatic (light blue), Conserved (orange), and Boundary (brown). The ACD boundaries are indicated by a light gray inset and the ACD edge groove is colored in dark gray. Ile-X-Ile motifs in the NTR Distal sub-region and CTR are indicated in purple.

bioRxiv preprint doi: https://doi.org/10.1101/2022.05.30.493970; this version posted May 30, 2022. The copyright holder for this preprint (which was not certified by peer review) is the author/funder, who has granted bioRxiv a license to display the preprint in perpetuity. It is made available under aCC-BY 4.0 International license.

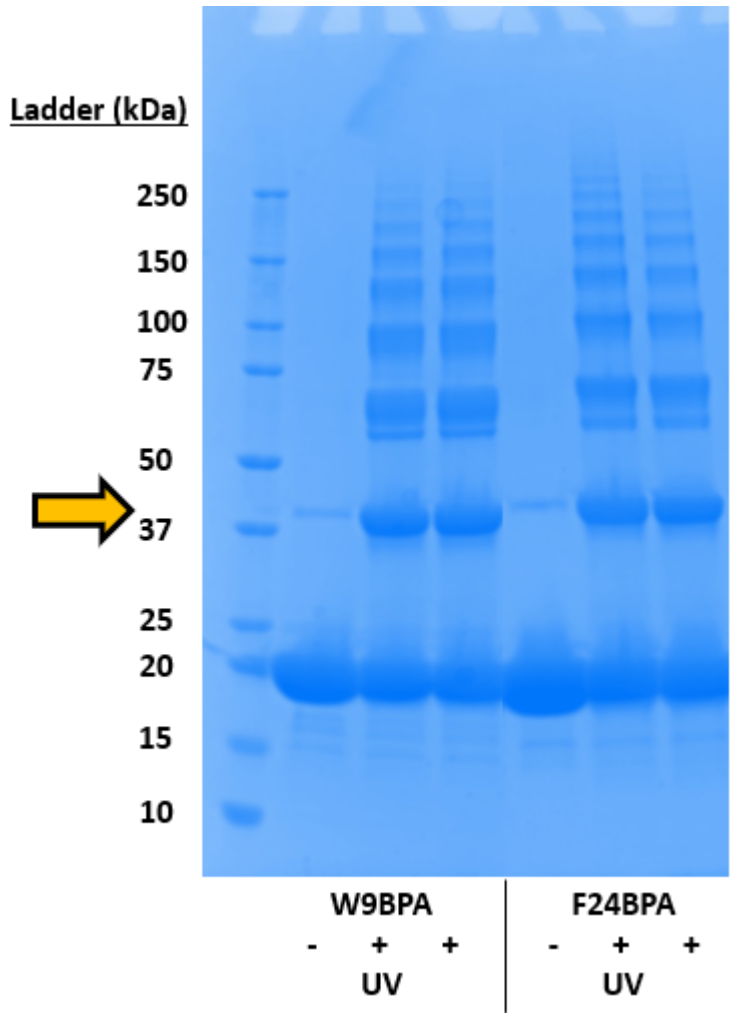

Figure 4-figure supplement 1. UV cross-linking reactions for HSPB5 BPA mutants W9BPA and F24BPA. HSPB5 BPA mutants were incubated at 4 °C with (+) or without (-) exposure to 360 nm UV light. The covalent HSPB5 dimer band (identified by gold arrow) was selected for in-gel digestion.

bioRxiv preprint doi: https://doi.org/10.1101/2022.05.30.493970; this version posted May 30, 2022. The copyright holder for this preprint (which was not certified by peer review) is the author/funder, who has granted bioRxiv a license to display the preprint in perpetuity. It is made available under aCC-BY 4.0 International license.

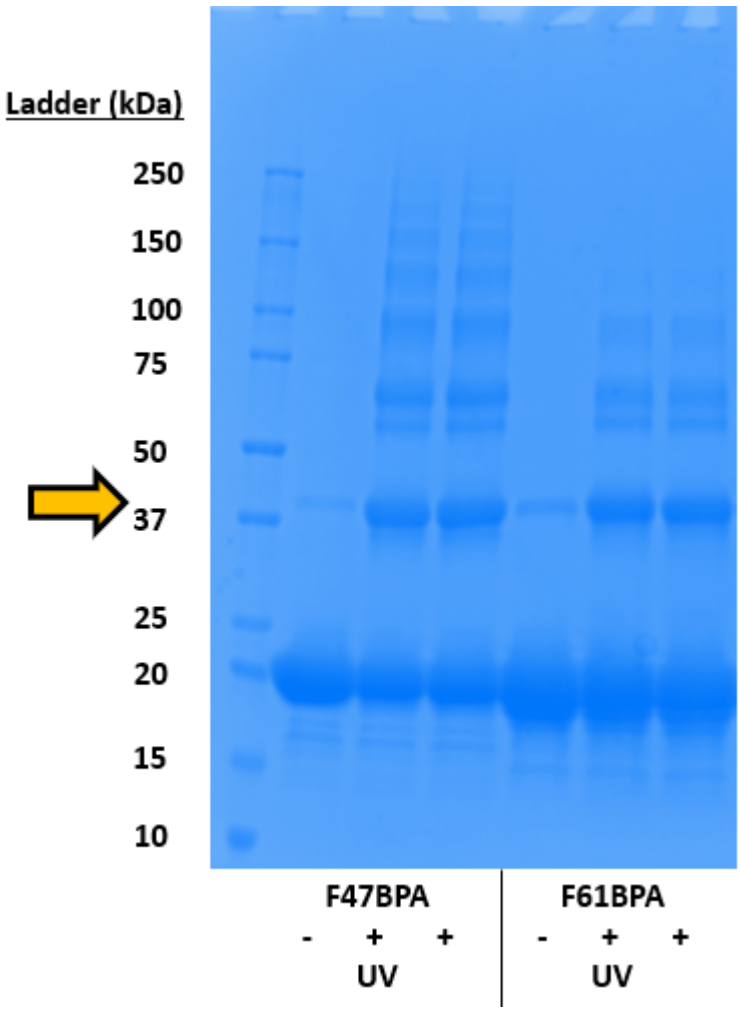

Figure 4-figure supplement 2. UV cross-linking reactions for HSPB5 BPA mutants F47BPA and F61BPA. HSPB5 BPA mutants were incubated at 4 °C with (+) or without (-) exposure to 360 nm UV light. The covalent HSPB5 dimer band (identified by gold arrow) was selected for in-gel digestion.

Discussion

Polydispersity and heterogeneity of human small heat shock proteins have long presented barriers to their structural and mechanistic understanding. Although polydisperse oligomers can in principle be parsed by single-particle cryo-EM, the level of heterogeneity within a given sized sHSP oligomer remains a substantial challenge (Kaiser et al., 2019). What gives rise to such heterogeneity and how does it relate to sHSP function? To address these fundamental questions, we have developed approaches that provide information regarding the heterogeneous oligomer ensembles holistically. Following the notion that sHSPs have evolved to perform their function under physiological conditions towards proteins expressed in the same tissues, we investigated a sHSP that is abundant in eye lens and a bona fide lens client, GammaD. Our efforts were guided by two inherited HSPB5 mutations associated with cataract under the presumption that these were likely loss-of-function or dominant negative mutations that lead to untimely protein aggregation in lens. Our findings reveal new insights into the

bioRxiv preprint doi: https://doi.org/10.1101/2022.05.30.493970; this version posted May 30, 2022. The copyright holder for this preprint (which was not certified by peer review) is the author/funder, who has granted bioRxiv a license to display the preprint in perpetuity. It is made available under aCC-BY 4.0 International license.

structure and function of HSPB5. First, HSPB5 distinguishes native GammaD from damaged GammaD even though the mutant/damaged GammaD is folded, consistent with recent reports that HSPB5 WT binds the destabilized GammaS-crystallin G18V mutant but not the function-preserving GammaS G18A mutant (Sprague-Piercy et al., 2020). Second, the heterogenous NTR is essential for HSPB5 chaperone activity towards GammaD, whereas the structured ACD has no intrinsic activity. A requirement for the NTR has previously been reported for an unfolded model client that forms amorphous aggregates (Mainz et al., 2015). Third, distinct sub-regions within the NTR interact with specific grooves presented on the ACD dimer and/or with other NTR sub-regions. Importantly, the number of binding partners is greater than the number of binding sites, leading to a large, but finite number of potential combinations of interactions within a given oligomer at any given time (Figure 5A). This situation was previously dubbed "quasi-order" and provides a way to describe the heterogeneity in HSPB5 as well as other sHSPs that exist as oligomers (Clouser et al., 2019).

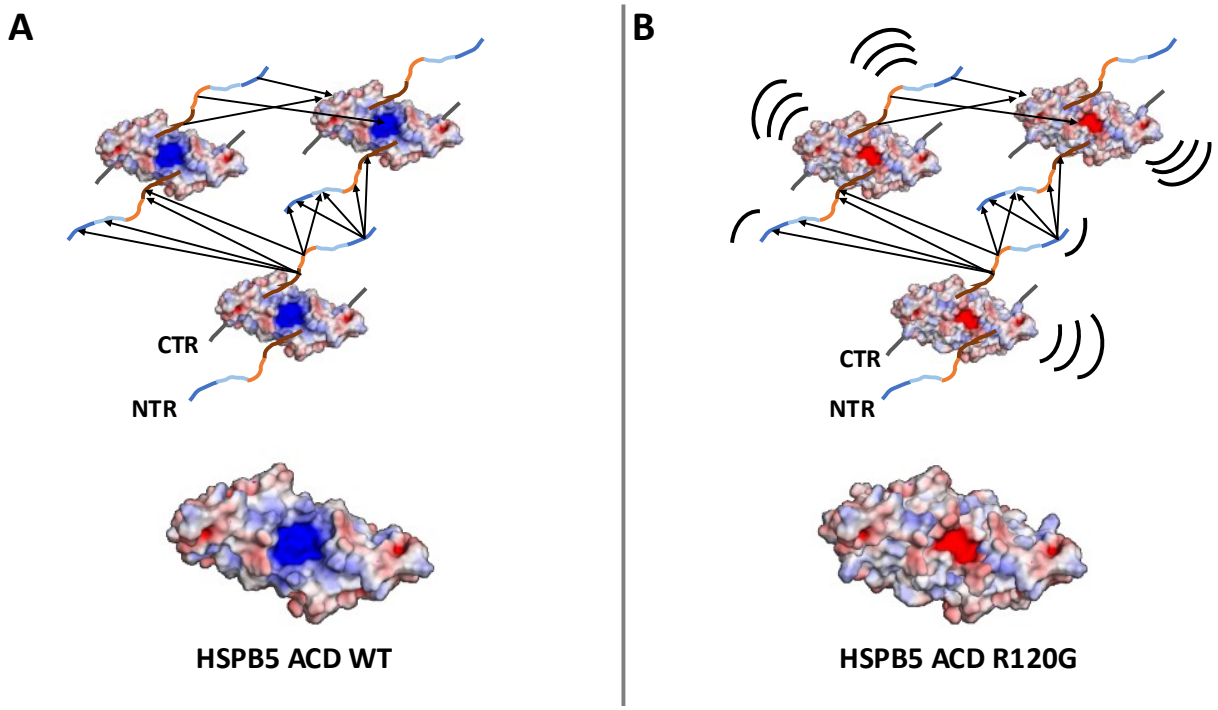

Figure 5. Summary of HSPB5 interactions and changes imparted by the R120G and D109H mutations. Specific NTR to NTR and NTR to ACD interactions (black arrows) determined for HSPB5 WT (A) and inferred for HSPB5 R120G (B). APBS electrostatics images are shown below for HSPB5 WT ACD-only (PDB: 2N0K) and R120G ACD-only (PDB: 6BP9) solution NMR ensembles, revealing a change in the central groove charge from positive to negative. The R120G and D109H mutations decrease structure and/or increase dynamics of the NTR and ACD (curved black lines).

How do changes in client interactions inform our understanding of cataract and myopathy development associated with inherited HSPB5 mutations? Previous work revealed increased interactions between HSPB5 R120G and muscle client desmin that affected client filament network status and mechanical properties in cells and in vitro (Perng et al., 2004; Wang et al., 2001). We observed formation of long-lived, high molecular weight co-complexes of HSPB5 and its lens client,

bioRxiv preprint doi: https://doi.org/10.1101/2022.05.30.493970; this version posted May 30, 2022. The copyright holder for this preprint (which was not certified by peer review) is the author/funder, who has granted bioRxiv a license to display the preprint in perpetuity. It is made available under aCC-BY 4.0 International license.

GammaD W130E. Mutant HSPB5 oligomers bind GammaD under conditions where HSPB5 WT does not, resulting in higher apparent chaperone activity under lab conditions where aggregation occurs on a timescale of minutes-to-hours. Furthermore, there is a continual uptake of client over time and this occurs more rapidly and more readily for the mutant HSPB5 species. Extrapolating such behavior to the situation in lens where the lack of protein synthesis means there is a fixed and finite amount of chaperone present over an individual's lifetime, the "more effective" HSPB5 mutants may reach their capacity limit faster than the "less effective" WT chaperone or may interact differently with other lens client proteins. The progressive uptake of GammaD by HSPB5 has parallels to age-dependent changes in wild-type mouse lens that occur over a lifetime of accumulated damage (Kaiser et al., 2019). All lens proteins, including HSPB5, are found in aggregates in cataractous lenses, suggesting similar processes occur *in vivo* (MacCoss et al., 2002). In lens, HSPB5 is associated with the lens sHSP HSPB4, forming mixed oligomers. Further studies will be needed to address interactions between HSPB4 and GammaD and how mixed oligomer formation affects these interactions. Expression of HSPB4, βA2-crystallin, or GammaD cataract-associated mutants in mice revealed similar changes in the proteome in all cases, which suggested the eye lens requires a delicate balance of interactions to maintain spatial order required for lens transparency (Kaiser et al., 2019). Our data indicate HSPB5 R120G and D109H form increased client interactions and support the chaperone capacity model of cataract formation.

Ideas and Speculation

Since its discovery in 1998, many studies have been conducted with the goal of understanding how HSPB5 R120G leads to cataract and myopathy. Our results reveal that the R120G and D109H disease-associated mutants are activated chaperones towards the lens client GammaD and can interact productively under conditions where HSPB5 WT cannot (pH 7.5). Consistent with that phenotype, the NTRs are less protected from hydrogen/deuterium exchange and, hence, more available for interaction with client in mutant oligomers. How can sequence changes in the ACD affect the states of the NTR and thus client engagement? Identification of HSPB5 NTR sub-regions that interact with grooves in the ACD provides a plausible direct connection. In particular, a sub-region that contains the only conserved sequence among human sHSP NTRs has now been reported to interact with the central ACD groove in HSPB5 (this work), HSPB1 (Clouser et al., 2019), and HSPB6 (Sluchanko et al., 2017). Solution NMR structures of the HSPB1 and HSPB5 WT ACD-only dimers display a central groove that is electrostatically positive (Figure 5A; PDB 2N3J, 2N0K; Rajagopal et al., 2015a; Rajagopal et al., 2015b). In stark contrast, solution NMR structures of the HSPB5 R120G ACD-only dimer display a smaller, less pronounced central groove that is electrostatically negative (Figure 5B; P. Rajagopal, PDB 6BP9). The large change is due to a shift in the register of the anti-parallel strands that compose the dimer interface, including the strand that contains R120. Notably, in the only crystal structure of full-length human HSPB6, the conserved NTR sequence, –SRLFDQ–, is inserted with the conserved aspartic acid pointing into the ACD central groove (Sluchanko et al., 2017; PDB 5LTW). Strong conservation of negative charge in the Conserved NTR sub-region suggests this could be a key regulatory interaction among sHSPs (Figure 1-figure supplement 3). We propose that the changes in the central groove due to the R120G mutation provide a structural rationale for the loss of interaction between the Conserved NTR sub-region and the ACD central groove. Although there is currently no structure available for the D109H ACD-only dimer, the concordance of observations between the two mutants suggests that a similar situation occurs for this mutant as well.

Changes in NTR structure/dynamics are not limited to sub-regions that bind the ACD. Based on the network of NTR-NTR interactions observed by BPA crosslinking, we propose that loss of any

bioRxiv preprint doi: https://doi.org/10.1101/2022.05.30.493970; this version posted May 30, 2022. The copyright holder for this preprint (which was not certified by peer review) is the author/funder, who has granted bioRxiv a license to display the preprint in perpetuity. It is made available under aCC-BY 4.0 International license.

individual interaction, such as the Conserved/central groove interaction, perturbs the entire network. Indeed, with one exception, all NTR sub-regions are less protected from HDX in mutant oligomers. The Distal NTR interacts via a knob-into-hole interaction with the ACD edge groove and our HDX data suggest that this interaction is maintained in the mutant oligomers. Extensive perturbation of the NTR is an expected consequence of "quasi-order" and was first observed in human HSPB1, where mutations in the Conserved or Boundary NTR sub-regions affected HDX in the opposite sub-region (Clouser et al., 2019). A relationship between these NTR sub-regions was also observed in BS3 cross-linking experiments on HSPB4 (Kaiser et al., 2019) as well as in our targeted BPA cross-linking experiments, suggesting this interaction may be a common feature of sHSPs.

A model in which loss or change in an NTR interaction alters the entire network of quasi-ordered interactions may provide a means to understand other disease-associated mutations in HSPB5 and other sHSPs. There are numerous mutations of ACD residues that cluster near the central groove. The peculiar sequence of the HSPB5 ACD central groove (which is highly conserved among other human sHSPs) results in a delicate balance of charged, polar, and hydrophobic interactions that span the ACD surface and are highly interdependent. Chemical changes at any single site from mutation, modification, or damage are expected to affect the entire network. Consistent with this idea, phosphorylation of yeast Hsp26 ACD affects availability of its NTR for client interactions (Mühlhofer et al., 2021). Identification of NTR-to-ACD and NTR-to-NTR interactions and experimental approaches that can detect these provide a way to understand the effects of such mutations on sHSP structure and function. The work here, along with previous studies of human HSPB1, establish a framework for describing quasi order of polydisperse and heterogenous small heat shock proteins and investigating their functional consequences.

Materials and Methods

Growth and purification of HSPB5 WT and mutants

E. coli BL21 cells were transformed with HSPB5 WT or mutants in a pET23 vector. Cells were grown to an OD600 of 0.6 at 37 °C while shaking at 200 RPM, then adjusted to 22 °C and induced by addition of 1 mM IPTG. BPA was site-specifically incorporated in HSPB5 amber codon mutants by co-expression with pEVOL-pBpF. pEVOL-pBpF was a gift from Peter Schultz (Addgene plasmid # 31190 ; http://n2t.net/addgene:31190 ; RRID:Addgene_31190). HSPB5 BPA mutant cells were cultured identically to HSPB5 WT following induction by 1 mM IPTG and 1 mM Arabinose. After growing overnight, cells were harvested and resuspended in 20 mM Tris, 100 mM NaCl, 10 mM EDTA pH 8. Cells were treated with DNase, RNase, and lysozyme and were subsequently lysed using a french press. PEI (0.1%) was added to the cell lysate and then clarified by centrifugation. The supernatant was retained and was adjusted to 31.5% ammonium sulfate (w/v) and clarified by centrifugation at 17k RPM for 20 minutes. The ammonium sulfate pellet contains HSPB5 and was retained for purification. The ammonium sulfate pellet was solubilized in 20 mM Tris pH 8 and applied to a G25 desalting column equilibrated in 20 mM Tris pH 8. Desalted protein eluted from the G25 column was applied to a DEAE column equilibrated in 20 mM Tris pH 8 and eluted with 20 mM Tris, 100 mM NaCl pH 8. Protein eluted from the DEAE column was diluted at least 2-fold in 20 mM Tris pH 8 and then applied to HiTrap Q columns (Cytiva, 10 mL bed volume) and eluted by a sodium chloride gradient from 0-300 mM over 8 column volumes. Protein eluted from the Q column was concentrated to 2 mL and then applied to a 120

bioRxiv preprint doi: https://doi.org/10.1101/2022.05.30.493970; this version posted May 30, 2022. The copyright holder for this preprint (which was not certified by peer review) is the author/funder, who has granted bioRxiv a license to display the preprint in perpetuity. It is made available under aCC-BY 4.0 International license.

mL SDX200 column equilibrated in 25 mM NaPO4, 150 mM NaCl pH 7.5. The same procedure was used for the HSPB5 ACD-CTR and ACD-only constructs, except a 120 mL SDX75 column was used for the final step.

Growth and purification of GammaD-crystallin

GammaD-crystallin was expressed in *E. coli* BL21 cells as a C-terminal HexaHis-Sumo fusion in pET28a vector. After reaching an OD600 of 0.6 at 37 °C, temperature was adjusted to 20 °C and cells were induced with 0.5 mM IPTG and grown overnight. Cells were harvested and resuspended in 25 mM Tris, 200 mM NaCl, 10 mM imidazole pH 7.6, treated with DNase, RNase, and lysozyme, and lysed using a french press. PEI (0.1%) was added to the cell lysate and then clarified by centrifugation at 20k RPM for 20 minutes. The supernatant was applied to HisTrap columns (Cytiva) equilibrated in 25 mM Tris, 200 mM NaCl, 10 mM imidazole pH 7.6. His-Sumo-GammaD was eluted from the column using 25 mM Tris, 200 mM NaCl, 500 mM imidazole pH 7.6. GST-SENP1 protease was added to the eluted protein and the mixture was dialyzed in 20 mM Tris, 200 mM NaCl, 10 mM imidazole, 2 mM β-mercaptoethanol pH 7.6 overnight at 4 °C. Cleaved protein was re-applied to a HisTrap column equilibrated in 25 mM Tris, 200 mM NaCl, 10 mM imidazole pH 7.6 and the flowthrough was concentrated and then applied to a 120 mL SDX75 column equilibrated in 20 mM Tris, 50 mM NaCl, 5 mM EDTA, 5 mM BME pH 8. Fractions containing GammaD were concentrated and then stored in 25 mM NaPO4, 150 mM NaCl, 0.1 mM EDTA pH 6.5 or 7.5.

Chaperone Activity Assay

Chaperone activity assays were conducted in a 96 well flat-bottom half-area plate with a final volume of 100 µL. GammaD-crystallin was adjusted to a concentration of 1 mM and incubated on ice. Assay wells containing HSPB5 in 25 mM NaPO4, 150 mM NaCl (or buffer only) in 50 µL total volume were pre-heated for 5 minutes at 37 °C. Following pre-heating, 50 µL ice cold GammaD W130E in 25 mM NaPO4, 150 mM NaCl, 0.1 mM EDTA was added. The plate was incubated at 37 °C and A360 measurements were taken once per minute, with 5 seconds of shaking before each measurement.

Nuclear Magnetic Resonance Spectroscopy

HSPB5 WT ACD was enriched with 15N by growing in minimal media supplemented with 15N-ammonium chloride and purified as described previously. HSPB5 NTR-derived synthetic peptides were purchased from Genscript. All peptides were produced with N-terminal formylation and C-terminal amidation, except for the Distal NTR peptide (HSPB5 residues 1-13) which had an amidated C-terminus and an unmodified N-terminus. Peptides were dissolved in 16.67-100% deuterated DMSO, depending on solubility, and titrated into 15N-labelled HSPB5 WT ACD-only in 25 mM MOPS, 100 mM sodium chloride, pH 7.5 buffer containing 10% D2O. The concentration of d-DMSO in the final NMR samples was maintained below 1% to prevent perturbation of HSPB5 ACD-only. HSQC-TROSY NMR spectra were recorded at 295 kelvin on a Bruker 500 MHz Avance III spectrometer or on a 600 MHz Avance II spectrometer equipped with a cryoprobe. Spectra were processed and analyzed using NMRPipe/NMRDraw (Delaglio et al., 1995) and Sparky (Lee et al., 2015) and visualized with NMRView (Johnson, n.d.) in NMRBox (Maciejewski et al., 2017).

Hydrogen/Deuterium Exchange Mass Spectrometry

bioRxiv preprint doi: https://doi.org/10.1101/2022.05.30.493970; this version posted May 30, 2022. The copyright holder for this preprint (which was not certified by peer review) is the author/funder, who has granted bioRxiv a license to display the preprint in perpetuity. It is made available under aCC-BY 4.0 International license.

All samples were incubated at 37 °C for 3 hours in water-based buffer and then cooled to room temperature before undergoing deuterium exchange. HSPB5 WT and mutants (0.04 mg/mL) were incubated at room temperature in 85% D2O-based PBS pH 7.5 buffer for 4 seconds, 1 minute, 30 minutes, or 20 hours. Fully deuterated samples were made by incubating protein in 85% D2O buffer at 75 °C for 30 mins. Exchange was quenched by addition of ice-cold quench buffer (1.6% formic acid) and samples were flash frozen in liquid nitrogen. Samples were automatically thawed, digested by immobilized pepsin and AN-PEP (Tsitsiani et al., 2017), and injected on a Waters Synapt G2-Si instrument using a setup built in house around the LEAP PAL system (Watson et al., 2021). HSPB5 peptides were identified by MS/MS on a Thermo Orbitrap Fusion Tribrid instrument and MS^E on a Waters Synapt G2-Si followed by data analysis using ProteinProspector (UCSF) or ProteinLynx Global SERVER (Waters). Deuterium uptake was analyzed in HDExaminer 3.0 (Sierra Analytics) and HX-Express (Guttman et al., 2013).

BPA Crosslinking Mass Spectrometry

BPA was incorporated in HSPB5 using amber codon suppression technology (Chin et al., 2002). The amber codon was inserted at HSPB5 site 9, 24, 47, or 61 using QuikChange mutagenesis (Agilent). Single-BPA HSPB5 mutants were purified using the standard protocol while taking steps to limit exposure to ambient light. Sample concentrations were determined using BCA. 50 µM HSPB5 BPA mutants were incubated for 3 hours at 37 °C, cooled to 4 °C, placed in a 96-well flat-bottomed half-area plate, and then exposed to UV for 30 minutes at 4 °C. Samples were subjected to SDS-PAGE on a 4-20% acrylamide gradient gel (Bio-Rad). The no-UV monomer and plus-UV dimer bands were excised and were each digested in-gel with MS grade Trypsin (Thermo Scientific) and GluC (New England Biolabs) in ammonium bicarbonate buffer (Thermo Manual - In-Gel Tryptic Digestion Kit). Digests were cleaned up with C18 spin columns (Thermo Scientific) and dried using a speed-vac. Samples were resuspended in 95% water 5% ACN with 0.1% FA with volumes adjusted based on sample weight. Data was collected with an Easy Nano LC coupled to a Thermo Orbitrap Fusion Lumos Tribrid. 0.5 µg of protein was loaded onto an 8-cm trap column. The sample was then then separated on a 25-cm analytical column with a 75 µm inner diameter using an 85-minute gradient from 6% B to 45% B, where A was water and B was 80% acetonitrile, at 300 nL min^{-1}. The column was then flushed and regenerated for 35 minutes. Spectra were acquired across the entire LC method using data-dependent acquisition with dynamic exclusion after one time for a duration of 30 seconds and an intensity threshold of $2.0x10^4$. Orbitrap detection and Higher-energy C-trap dissociation (HCD) fragmentation (30% normalized collision energy) were used with a target value of $1.00x10^5$, maximum injection time of 22 ms, top N of 20, and isolation width of 1.6. MS1 were acquired at a resolution of 120,000 over the range of 400-2000 m/z, and MS2 were acquired with a resolution of 15,000. The mass spectrometry proteomics data have been deposited to the ProteomeXchange Consortium via the PRIDE partner repository (Perez et al., 2019) with the dataset identifier PXD034114.

Identification of Crosslinks Using the Trans Proteomic Pipeline (TPP)

First, Comet (Eng et al., 2013) was used to search for non-crosslinked peptides in the non-UV treated control to construct the protein database. The Comet search database contained the BL21 *E. coli* database from uniprot (UP000431028), the cRAP database from the Global Proteome Machine with all 5 levels of proteins (cRAP Protein Sequences), the pertinent HSPB5 BPA mutant, and reverse-sequence decoys. The Comet searches were enzyme nonspecific using a peptide mass tolerance of 20.0 ppm. The

bioRxiv preprint doi: https://doi.org/10.1101/2022.05.30.493970; this version posted May 30, 2022. The copyright holder for this preprint (which was not certified by peer review) is the author/funder, who has granted bioRxiv a license to display the preprint in perpetuity. It is made available under aCC-BY 4.0 International license.

isotope error offset was 3, and BPA was defined as an additional amino acid, B, that has a mass of 251.09462859 Da. Methionine oxidation and cysteine iodoacetamide alkylation were variable modifications. Results were validated using Peptide Prophet (Keller et al., 2002). After filtering using a 1% False Discovery Rate (FDR, based on PeptideProphet probabilities) and a minimum of 2 Peptide Spectral Match (PSM), this yields a protein database for the sample.

Second, crosslinks in the UV-treated samples were identified using Kojak (Hoopmann et al., 2015) and the protein database for the sample. The Kojak search settings matched those described for the Comet searches expect the precursor tolerance was 15 ppm and enzyme selection rules were used. For the trypsin digested samples, the preexisting trypsin setting was used. For the trypsin-GluC digested samples, the cleavage sites of D and E were added to the trypsin settings. Crosslinks were defined as from BPA to any residue with no mass change. Crosslink results were validated using PeptideProphet. For ions of each charge state, probabilities were determined using PeptideProphet and were used to define the thresholds used to filter results to a 1% FDR. For histograms, each PSM was associated with the residue that was assigned the highest probability of participating in a crosslink with BPA. When more than one residue was assigned the same probability, an equal fraction of that PSM was assigned to each of those residues.

Acknowledgements

We thank Edgar A. Hodge, Mark A. Benhaim, and Clint Vorauer for assistance with HDX feasibility studies and protease immobilization. We thank Daniele Canzani for assistance with early BPA cross-linking mass spectrometry experiments and Ponni Rajagopal for foundational studies on R120G-HSPB5 ACD. This work was supported by NIH grants R01 EY017370 to REK and R01 AI153191 to MG, and by T32 GM00826 to CNW, T32 GM007750 to EIJ, and T32 AG066574 to MKJ.

Competing Interests

The authors declare no competing interests.

References

Andley UP, Hamilton PD, Ravi N, Weihl CC. 2011. A Knock-In Mouse Model for the R120G Mutation of αB-Crystallin Recapitulates Human Hereditary Myopathy and Cataracts. *PLoS ONE* **6**:e17671. doi:10.1371/journal.pone.0017671

Bagnéris C, Bateman OA, Naylor CE, Cronin N, Boelens WC, Keep NH, Slingsby C. 2009. Crystal Structures of α-Crystallin Domain Dimers of αB-Crystallin and Hsp20. *The Journal of Molecular Biology* **392**:1242-1252. doi:10.1016/j.jmb.2009.07.069

Baldwin AJ, Lioe H, Hilton GR, Baker LA, Rubinstein JL, Kay LE, Benesch JLP. 2011. The Polydispersity of αB-Crystallin Is Rationalized by an Interconverting Polyhedral Architecture. *Structure* **19**:1855–1863. doi:10.1016/j.str.2011.09.015

bioRxiv preprint doi: https://doi.org/10.1101/2022.05.30.493970; this version posted May 30, 2022. The copyright holder for this preprint (which was not certified by peer review) is the author/funder, who has granted bioRxiv a license to display the preprint in perpetuity. It is made available under aCC-BY 4.0 International license.

Bassnett S, Duncan G. 1985. Direct measurement of pH in the rat lens using ion-sensitive microelectrodes. *Experimental Eye Research* **40**:585-590. doi:10.1016/0014-4835(85)90080-6

Boatz JC, Whitley MJ, Li M, Gronenborn AM, van der Wel PCA. 2017. Cataract-associated P23T γD-crystallin retains a native-like fold in amorphous-looking aggregates formed at physiological pH. *Nature Communications* **8**:15137. doi:10.1038/ncomms15137

Bova MP, Yaron O, Huang Q, Ding L, Haley DA, Stewart PL, Horwitz J. 1999. Mutation R120G in αB-crystallin, which is linked to a desmin-related myopathy, results in an irregular structure and defective chaperone-like function. *PNAS* **96**:6137-6142.

Brodehl A, Gaertner-Rommel A, Klauke B, Grewe SA, Schirmer I, Peterschröder A, Faber L, Vorgerd M, Gummert J, Anselmetti D, Schulz U, Paluszkiewicz L, Milting H. 2017. The novel αB-crystallin (CRYAB) mutation p.D109G causes restrictive cardiomyopathy. *Human Mutation* **38**:947–952. doi:10.1002/humu.23248

Chin JW, Martin AB, King DS, Wang L, Schultz PG. 2002. Addition of a photocrosslinking amino acid to the genetic code of Escherichia coli. *PNAS* **99:**11020-11024. doi:10.1073/pnas.172226299

Clark AR, Egberts WV, Kondrat FDL, Hilton GR, Ray NJ, Cole AR, Carver JA, Benesch JLP, Keep NH, Boelens WC, Slingsby C. 2018. Terminal Regions Confer Plasticity to the Tetrameric Assembly of Human HspB2 and HspB3. *The Journal of Molecular Biology* **430**:3297-3310. doi:10.1016/j.jmb.2018.06.047

Clouser AF, Baughman HER, Basanta B, Guttman M, Nath A, Klevit RE. 2019. Interplay of disordered and ordered regions of a human small heat shock protein yields an ensemble of 'quasi-ordered' states. *eLife* **8**:e50259. doi: 10.7554/eLife.50259

Datskevich PN, Nefedova VV, Sudnitsyna MV, Gusev NB. 2012. Mutations of small heat shock proteins and human congenital diseases. *Biochemistry Moscow* **77**:1500–1514. doi:10.1134/S0006297912130081

Delaglio F, Grzesiek S, Vuister GW, Zhu G, Pfeifer J, Bax A. 1995. NMRPipe: A multidimensional spectral processing system based on UNIX pipes. *Journal of Biomolecular NMR* **6**:277–293. doi:10.1007/BF00197809

Delbecq SP, Jehle S, Klevit RE. 2012. Binding determinants of the small heat shock protein, αB-crystallin: recognition of the 'IxI' motif. *EMBO* **31**:4587-4594. doi:10.1038/emboj.2012.318

Delbecq SP, Klevit RE. 2018. HSPB5 engages multiple states of a destabilized client to enhance chaperone activity in a stress-dependent manner. *The Journal of Biological Chemistry* **294**:3261-3270. doi:10.1074/jbc.RA118.003156

Dorman G, Prestwich GD. 1994. Benzophenone Photophores in Biochemistry. *Biochemistry* **33**:5661–5673. doi:10.1021/bi00185a001

Eng JK, Jahan TA, Hoopmann MR. 2013. Comet: An open-source MS/MS sequence database search tool. *Proteomics* **13**:22–24. doi:10.1002/pmic.201200439

bioRxiv preprint doi: https://doi.org/10.1101/2022.05.30.493970; this version posted May 30, 2022. The copyright holder for this preprint (which was not certified by peer review) is the author/funder, who has granted bioRxiv a license to display the preprint in perpetuity. It is made available under aCC-BY 4.0 International license.

Fichna JP, Potulska-Chromik A, Miszta P, Redowicz MJ, Kaminska AM, Zekanowski C. 2017. A novel dominant D109A CRYAB mutation in a family with myofibrillar myopathy affects αB-crystallin structure. *BBA Clinical* **7**:1-7. doi:10.1016/j.bbacli.2016.11.004

Fardeau M, Godet-Guillain J, Tome FMS, Collin H, Gaudeau S, Boffety C, Vernant P. 1978. Une nouvelle affection musculaire familiale, définie par l'accumulation intra-sarco-plasmique d'un matériel granulo-filamentaire dense en microscopie électronique. *Revue Neurologique* **134**:411-425.

Foster A. 2000. Vision 2020: The Cataract Challenge. *Community Eye Health Journal* **13**(34).

Ghosh JG, Clark JI. 2005. Insights into the domains required for dimerization and assembly of human αB crystallin. *Protein Science* **14**:684–695. doi:10.1110/ps.041152805

Guttman M, Weis DD, Engen JR, Lee KK. 2013. Analysis of Overlapped and Noisy Hydrogen/Deuterium Exchange Mass Spectra. *Journal of the American Society for Mass Spectrometry* **24**:1906–1912. doi:10.1007/s13361-013-0727-5

Hoopmann MR, Zelter A, Johnson RS, Riffle M, MacCoss MJ, Davis TN, Moritz RL. 2015. Kojak: Efficient Analysis of Chemically Cross-Linked Protein Complexes. *The Journal of Proteome Research* **14**:2190–2198. doi:10.1021/pr501321h

Horwitz J. 1992. α-Crystallin can function as a molecular chaperone. *PNAS* **89**:10449-10453.

Ingolia TD, Craig EA. 1982. Four small Drosophila heat shock proteins are related to each other and to mammalian α-crystallin. *PNAS* **79**:2360-2364.

Jehle S, van Rossum B, Stout JR, Noguchi SM, Falber K, Rehbein K, Oschkinat H, Klevit RE, Rajagopal P. 2009. αB-Crystallin: A Hybrid Solid-State/Solution-State NMR Investigation Reveals Structural Aspects of the Heterogeneous Oligomer. *Journal of Molecular Biology* **385**:1481–1497. doi:10.1016/j.jmb.2008.10.097

Jehle S, Vollmar BS, Bardiaux B, Dove KK, Rajagopal P, Gonen T, Oschkinat H, Klevit RE. 2011. N-terminal domain of αB-crystallin provides a conformational switch for multimerization and structural heterogeneity. *PNAS* **108**:6409–6414. doi:10.1073/pnas.1014656108

Johnson, B. A. (n.d.). Using NMRView to Visualize and Analyze the NMR Spectra of Macromolecules. In Protein NMR Techniques (pp. 313–352). *Humana Press* https://doi.org/10.1385/1-59259-809-9:313

Kaiser CJO, Peters C, Schmid PWN, Stavropoulou M, Zou J, Dahiya V, Mymrikov EV, Rockel B, Asami S, Haslbeck M, Rappsilber J, Reif B, Zacharias M, Buchner J, Weinkauf S. 2019. The structure and oxidation of the eye lens chaperone αA-crystallin. *Nature Structural and Molecular Biology* **26**:1141–1150. doi:10.1038/s41594-019-0332-9

Keller A, Nesvizhskii AI, Kolker E, Aebersold R. 2002. Empirical Statistical Model To Estimate the Accuracy of Peptide Identifications Made by MS/MS and Database Search. *Analytical Chemistry* **74**:5383–5392. doi:10.1021/ac025747h

bioRxiv preprint doi: https://doi.org/10.1101/2022.05.30.493970; this version posted May 30, 2022. The copyright holder for this preprint (which was not certified by peer review) is the author/funder, who has granted bioRxiv a license to display the preprint in perpetuity. It is made available under aCC-BY 4.0 International license.

Klevit RE. 2020. Peeking from behind the veil of enigma: emerging insights on small heat shock protein structure and function. *Cell Stress and Chaperones* **25**:573–580. doi:10.1007/s12192-020-01092-2

Koteiche HA, Mchaourab HS. 2006. Mechanism of a Hereditary Cataract Phenotype: mutations in αA-crystallin activate substrate binding. *The Journal of Biological Chemistry* **281**:14273-14279. doi:10.1074/jbc.M512938200

Leem CH, Lagadic-Gossmann D, Vaughan-Jones RD. 1999. Characterization of intracellular pH regulation in the guinea-pig ventricular myocyte. *The Journal of Physiology* **517**:159–180. doi:10.1111/j.1469-7793.1999.0159z.x

Liang JJ, Liu B-F. 2006. Fluorescence resonance energy transfer study of subunit exchange in human lens crystallins and congenital cataract crystallin mutants. *Protein Science* **15**:1619–1627. doi:10.1110/ps.062216006

Lynnerup N, Kjeldsen H, Heegaard S, Jacobsen C, Heinemeier J. 2008. Radiocarbon Dating of the Human Eye Lens Crystallines Reveal Proteins without Carbon Turnover throughout Life. *PLoS ONE* **3**:e1529. doi:10.1371/journal.pone.0001529

MacCoss MJ, McDonald WH, Saraf A, Sadygov R, Clark JM, Tasto JJ, Gould KL, Wolters D, Washburn M, Weiss A, Clark JI, Yates JR. 2002. Shotgun identification of protein modifications from protein complexes and lens tissue. *PNAS* **99**:7900–7905. doi:10.1073/pnas.122231399

Maciejewski MW, Schuyler AD, Gryk MR, Moraru II, Romero PR, Ulrich EL, Eghbalnia HR, Livny M, Delaglio F, Hoch JC. 2017. NMRbox: A Resource for Biomolecular NMR Computation. *Biophysical Journal* **112**:1529-1534. doi:10.1016/j.bpj.2017.03.011

Mainz A, Peschek J, Stavropoulou M, Back KC, Bardiaux B, Asami S, Prade E, Peters C, Weinkauf S, Buchner J, Reif B. 2015. The chaperone αB-crystallin uses different interfaces to capture an amorphous and an amyloid client. *Nature Structural and Molecular Biology* **22**:898–905. doi:10.1038/nsmb.3108

Mathias RT, Riquelme G, Rae JL. 1991. Cell to cell communication and pH in the frog lens. *Journal of General Physiology* **98**: 1085-1103. doi:10.1085/jgp.98.6.1085

Mühlhofer M, Peters C, Kriehuber T, Kreuzeder M, Kazman P, Rodina N, Reif B, Haslbeck M, Weinkauf S, Buchner J. 2021. Phosphorylation activates the yeast small heat shock protein Hsp26 by weakening domain contacts in the oligomer ensemble. *Nature Communications* **12**:6697. doi:10.1038/s41467-021-27036-7

Pedersen JT, Heegaard NHH. 2013. Analysis of Protein Aggregation in Neurodegenerative Disease. *Analytical Chemistry* **85**:4215–4227. doi:10.1021/ac400023c

Perez-Riverol Y, Csordas A, Bai J, Bernal-Llinares M, Hewapathirana S, Kundu DJ, Inuganti A, Griss J, Mayer G, Eisenacher M, Pérez E, Uszkoreit J, Pfeuffer J, Sachsenberg T, Yılmaz Ş, Tiwary S, Cox J, Audain E, Walzer M, Jarnuczak AF, Ternent T, Brazma A, Vizcaíno JA. 2019. The PRIDE database and

bioRxiv preprint doi: https://doi.org/10.1101/2022.05.30.493970; this version posted May 30, 2022. The copyright holder for this preprint (which was not certified by peer review) is the author/funder, who has granted bioRxiv a license to display the preprint in perpetuity. It is made available under aCC-BY 4.0 International license.

related tools and resources in 2019: improving support for quantification data. *Nucleic Acids Research* **47**:D442–D450. doi:10.1093/nar/gky1106

Perng MD, Wen SF, van den Ijssel P, Prescott AR, Quinlan RA. 2004. Desmin Aggregate Formation by R120G αB-Crystallin Is Caused by Altered Filament Interactions and Is Dependent upon Network Status in Cells. *Molecular Biology of the Cell* **15**:2335-2346. doi:10.1091/mbc.e03-12-0893

Peschek J, Braun N, Rohrberg J, Back KC, Kriehuber T, Kastenmüller A, Weinkauf S, Buchner J. 2013. Regulated structural transitions unleash the chaperone activity of αB-crystallin. *PNAS* E3780-E3789. doi:10.1073/pnas.1308898110

Rajagopal P, Tse E, Borst AJ, Delbecq SP, Shi L, Southworth DR, Klevit RE. 2015. A conserved histidine modulates HSPB5 structure to trigger chaperone activity in response to stress-related acidosis. *eLife* **4**:e07304. doi:10.7554/eLife.07304

Rajagopal P, Liu Y, Shi L, Clouser AF, Klevit RE. 2015. Structure of the α-crystallin domain from the redox-sensitive chaperone, HSPB1. *Journal of Biomolecular NMR* **63**:223–228. doi:10.1007/s10858-015-9973-0

Sacconi S, Féasson L, Antoine JC, Pécheux C, Bernard R, Cobo AM, Casarin A, Salviati L, Desnuelle C, Urtizberea A. 2012. A novel CRYAB mutation resulting in multisystemic disease. *Neuromuscular Disorders* **22**:66-72. doi:10.1016/j.nmd.2011.07.004

Serebryany E, Takata T, Erickson E, Schafheimer N, Wang Y, King JA. 2016. Aggregation of Trp > Glu point mutants of human gamma-D crystallin provides a model for hereditary or UV-induced cataract. *Protein Science* **25**:1115–1128. doi:10.1002/pro.2924

Sluchanko NN, Beelen S, Kulikova AA, Weeks SD, Antson AA, Gusev NB, Strelkov SV. 2017. Structural Basis for the Interaction of a Human Small Heat Shock Protein with the 14-3-3 Universal Signaling Regulator. *Structure* **25**:305-316. doi:10.1016/j.str.2016.12.005

Sprague-Piercy MA, Wong E, Roskamp KW, Fakhoury JN, Freites JA, Tobias DJ, Martin RW. 2020. Human αB-crystallin discriminates between aggregation-prone and function-preserving variants of a client protein *BBA General Subjects* doi:10.1016/j.bbagen.2019.129502

Treweek TM, Rekas A, Lindner RA, Walker MJ, Aquilina JA, Robinson CV, Horwitz J, Der Perng M, Quinlan RA, Carver JA. 2005. R120G αB-crystallin promotes the unfolding of reduced α-lactalbumin and is inherently unstable. *The FEBS Journal* **272**:711–724. doi:10.1111/j.1742-4658.2004.04507.x

Tsiatsiani L, Akeroyd M, Olsthoorn M, Heck AJR. 2017. *Aspergillus niger* Prolyl Endoprotease for Hydrogen–Deuterium Exchange Mass Spectrometry and Protein Structural Studies. *Analytical Chemistry* **89**:7966–7973. doi:10.1021/acs.analchem.7b01161

Vicart P, Caron A, Guicheney P, Li Z, Prévost M-C, Faure A, Chateau D, Chapon F, Tomé F, Dupret J-M, Paulin D, Fardeau M. 1998. A missense mutation in the αB-crystallin chaperone gene causes a desmin-related myopathy. *Nature Genetics* **20**:92–95. doi:10.1038/1765

bioRxiv preprint doi: https://doi.org/10.1101/2022.05.30.493970; this version posted May 30, 2022. The copyright holder for this preprint (which was not certified by peer review) is the author/funder, who has granted bioRxiv a license to display the preprint in perpetuity. It is made available under aCC-BY 4.0 International license.

Wang X, Osinska H, Klevitsky R, Gerdes AM, Nieman M, Lorenz J, Hewett T, Robbins J. 2001. Expression of R120G–αB-Crystallin Causes Aberrant Desmin and αB-Crystallin Aggregation and Cardiomyopathy in Mice. *Circulation Research* **89**:84-91. doi:10.1161/hh1301.092688

Watson MJ, Harkewicz R, Hodge EA, Vorauer C, Palmer J, Lee KK, Guttman M. 2021. Simple Platform for Automating Decoupled LC–MS Analysis of Hydrogen/Deuterium Exchange Samples. *Journal of the American Society for Mass Spectrometry* **32**:597–600. doi:10.1021/jasms.0c00341

Wu S-Y, Zou P, Mishra S, Mchaourab HS. 2018. Transgenic zebrafish models reveal distinct molecular mechanisms for cataract-linked αA-crystallin mutants. *PLoS ONE* **13**:e0207540. doi:10.1371/journal.pone.0207540